Finite element skin models as additional data for dynamic infrared thermography on skin lesions

Quantitative InfraRed Thermography Journal

Finite element skin models as additional data for dynamic infrared thermography on skin lesions

--Manuscript Draft--

Full Title:	Finite element skin models as additional data for dynamic infrared thermography on skin lesions
Manuscript Number:	TQRT-2023-0024R2
Article Type:	Research Article
Keywords:	Finite element model; skin cancer; dynamic infrared thermography; data augmentation; FEM
Abstract:	Skin cancer is a significant global health concern, with increasing incidence rates and a high number of deaths each year. Early detection plays a crucial role in improving survival rates, but current screening methods, such as total body skin examination, often lead to unnecessary invasive excisions. This research aims to explore the use of dynamic infrared thermography (DIRT) in combination with other technologies to potentially eliminate the need for biopsies in the future and gather information about the stage or depth of malignant skin lesions. This article focuses on using DIRT in skin cancer diagnostics and presents a proof-of-concept study conducted at the University of Antwerp. The study involves data acquisition using a thermal camera and a finite element skin model. The FEM skin model employed in this research follows the commonly used five-layer model. Each layer is assigned specific thermophysical properties such as thermal conductivity, blood perfusion rate, and thickness. While the FEM skin model shares certain similarities with the measurement data, there is room for further enhancements to optimize its performance. The acquired data is analyzed to assess the effectiveness of the combined technique compared to existing clinical and diagnostic methods.
Order of Authors:	Jan Verstockt
	Ruben Somers
	Filip Thiessen
	Isabelle Hoorens
	Lieve Brochez
	Gunther Steenackers
Response to Reviewers:	I added a 'Rebuttal_REV3.pdf' file with the responds to the reviewers.

Finite element skin models as additional data for dynamic infrared thermography on skin lesions

by Jan Verstockt[*], Ruben Somers[*], Filip Thiessen[**], Isabelle Hoorens[***], Lieve Brochez[***], Gunther Steenackers[*]

[*] *InViLab Research Group, University of Antwerp, Groenenborgerlaan 171, B-2020 Antwerp, Belgium*
[**] *Department of Plastic, Reconstructive and Aesthetic Surgery, Multidisciplinary Breast Clinic, Antwerp University Hospital, University of Antwerp, Wilrijkstraat 10, B-2650 Antwerp, Belgium*
[***] *Department of Dermatology, Ghent University Hospital, C. Heymanslaan 10, B-9000 Ghent, Belgium*

Abstract

Skin cancer is a significant global health concern, with increasing incidence rates and a high number of deaths each year. Early detection plays a crucial role in improving survival rates, but current screening methods, such as total body skin examination, often lead to unnecessary invasive excisions. This research aims to explore the use of dynamic infrared thermography (DIRT) in combination with other technologies to potentially eliminate the need for biopsies in the future and gather information about the stage or depth of malignant skin lesions. This article focuses on using DIRT in skin cancer diagnostics and presents a proof-of-concept study conducted at the University of Antwerp (Belgium). The study involves data acquisition using a thermal camera and a finite element skin model. The FEM skin model employed in this research follows the commonly used five-layer model. Each layer is assigned specific thermophysical properties such as thermal conductivity, blood perfusion rate, and thickness. A FEM skin model in Siemens Simcenter 3D is constructed to be able to simulate the cryogenic cooling on the skin. It is possible to improve the thermal images by choosing an appropriate cooling method, cooling sequence and optimized measurement setup. While the FEM skin model shares certain similarities with the measurement data, there is room for further enhancements to optimize its performance. The acquired data is analyzed to assess the effectiveness of the combined technique compared to existing clinical and diagnostic methods.

Keywords: Finite element model, skin cancer, dynamic infrared thermography, data augmentation, FEM, Pennes

1. Introduction

1.1 Skin Cancer

Cancer is a significant global health concern, with an estimated annual toll of almost 10 million deaths and more than 19 million new cases worldwide [1]. The incidence rates of melanoma, a type of skin cancer, have tripled in Europe and the United States over the past four decades [1], [2]. Nonmelanoma skin cancer, contributes to over one million new cases (1,198,073 or 11% of estimated new cases in 2020, worldwide for both sexes and all ages) and 64,000 (0.6%) deaths each year globally. Men are affected at a rate twice as high as women. Melanoma skin cancer accounts for more than 324,635 (3.4% of estimated new cases in 2020, worldwide for both sexes and all ages) new cases and approximately 60,000 (0.6%) deaths annually [1].

Skin cancer encompasses various pathological conditions arising from different cell types in the epidermis and dermis. It is primarily categorized into melanoma and non-melanoma skin cancer, with the latter mainly comprising keratinocyte cancers (basal and squamous cell carcinomas) and rarer types like Merkel cell carcinoma[1], [2]. Early detection plays a crucial role in improving survival rates and enabling more effective and cost-efficient treatments with minimal impact on patients' quality of life [3]. Regular screening is recommended for specific high-risk populations, such as annual breast cancer screening for older women and annual lung cancer screening for individuals aged 55 to 74 with a history of smoking [4], [5]. Presently, a total body skin examination (TBSE) is the commonly used screening method [4]. Dermatologists perform this inexpensive and non-invasive procedure to identify potential malignant and benign skin lesions. The accuracy of their diagnoses is influenced by their training and experience [6]. Trained dermatologists can enhance accuracy by incorporating polarized light dermoscopy, which highlights additional features like pigmentation or vascularization [7], [8]. However, invasive excisions are still conducted to rule out false-negative findings that could lead to metastasis and death. Unfortunately, many of these excisions are unnecessary, as only one melanoma is detected for every 10 to 60 biopsies performed [9], [10].

The purpose of this research is to explore the use of dynamic infrared thermography, in combination with technologies such as finite element (FEM) models of the human skin, digital dermoscopy and hyperspectral imaging (the latter two are not in the scope of this article), to potentially eliminate the need for biopsies in the future. Additionally in future work, the aim is to gather information about the stage or depth of malignant skin lesions. This information can assist surgeons in accurately removing the malignant skin lesion by detecting the subcutaneous area.

1.2 Dynamic infrared thermography in biomedical applications

The use of infrared thermal imaging in biomedical applications was uncommon in the past. The bulky first-generation IR cameras and their limited performance together with the unsatisfactory results of passive thermography are the root cause [11]–[13] . Active dynamic thermography and the problems to implement it in medical diagnostics has been extensively discussed by Nowakowski et al. [14]. Infrared thermography has been continuously improved over the last years and is recently widely used in biomedical applications for the detection of breast cancer, psoriasis, fever screening, dentistry or measuring flap perfusion during breast reconstruction with DIEP flaps [15]–[19] or even in cardiosurgery and the detection of blood vessels [20], [21]. Also body part and pose estimation based on medical thermographic images has been researched[22]. A full review on infrared thermography on skin cancer is out of the scope of this article but can be found in previous contributions [23], [24].

Recent additions to literature on the detection of cancers with infrared thermography are mostly based on a combination of artificial intelligence (AI) and numerical models with infrared thermography. Magalhaes et al. conducted research on the role of different AI classifiers in skin cancers images, not only limited to infrared thermography [25]. In the following work they did a comparison of the application of machine learning strategies for infrared thermography of skin cancer [26], [27]. Chen et al. trained an AI model on data generated by a 3D FEM model to extract the thermophysical properties of the skin cancer [28].

1.2.1 Skin cancer diagnosis using thermography – working principle

Biomedical infrared thermography reveals the heterogeneous skin and superficial tissue temperature [29]. Infrared emissions from human skin at 27 °C are in the wavelength range of 2–20 μm , and peaks at 10 μm. The term body infrared rays, a narrow wavelength range of 8–12 μm, is used for medical applications [30]. As reported by Lee and Minkina, the commonly accepted emissivity ϵ of human skin, independent of the skin pigmentation, is 0.98 ± 0.01 for $\lambda > 2$ μm, which makes human skin a close to perfect black body [13], [31]–[33].

As a living organism, the human body attempts to maintain homeostasis, the balance of all systems in the body, for all physiological processes, resulting in dynamic changes in heat output [3]. The result of a complicated combination of central and local regulatory systems is reflected in the surface temperature of an extremity. Core body temperature is maintained constant at depths greater than 20 mm [33]. Skin surface temperature is a useful indicator of health problems or physical disorders of skin-related processes [33]. Skin cancer cells are different compared to normal skin cells due to the high rate of uncontrolled cell division [34]. As a result of the high rate of cell division, cancer cells need to convert more energy to support the cellular processes. Due to the high metabolic rate, there is a higher energy demand, which also leads to increased angiogenesis. Angiogenesis is the physiological process by which new blood vessels form from existing vessels to provide the necessary additional energy [35], [36]. In conjunction with the increased energy requirements, melanoma skin lesions are thought to have a higher temperature (Δ 2–4 K) than the surrounding healthy skin [33], [37], [38].The IR imaging of melanoma skin lesions is based on the detection of new blood vessels and chemical changes associated with a tumour development and growth [39]. Currently, there is no standardized, reliable, quantitative, and non-invasive method based on IRT to accurately determine the malignant potential of skin lesions [10].

1.3 Finite element skin model

IR imaging combined with a mathematical model is used to understand the temporal evolution and time constants of the process [40]. This is a challenging task due to the many parameters of the Pennes's bioheat Equation (see section 1.3.1). Not only differ the thermophysical parameters from patient to patient but also the dimensions and position of the lesions, as well as the lesion parameters are patient dependant [41]. The Pennes bioheat Equation is not only used to study cancers of the skin [42]–[47] but also for simulating breast tumor analysis [28], [48]. The five-layer model is most commonly used to determine the temperature distribution during cooling. This model consists of the epidermis, papillary dermis, reticular dermis, subcutaneous fat and muscle. The FEM model implements the Pennes bioheat Equation. The parameters of the five layers used in the Pennes' bioheat Equation are shown in Table 1 and Table 2. With a mathematical model, the excitation method (cooling of the skin) can be analysed. The model can be used to conduct a parameter sensitivity study to gain understanding of the human skin

system. Cëtingul and Herman discovered that the thermal response of a lesion is mainly influenced by its total volume, average equivalent diameter, and penetration depth (stage), while small protrusions and irregularities have a relatively minor effect [40]. Cëtingul and Herman evaluated the effects of variations in thermophysical properties, metabolic heat generation, blood perfusion rate, and skin layer thickness on the distribution of surface temperatures, skin layers are tested and subjected to cooling and subsequent thermal recovery.

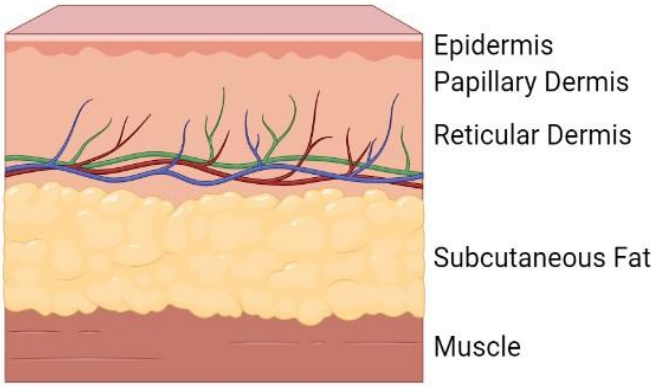

Figure 1- The 5-layer skin model consists of the epidermis, papillary dermis, reticular dermis, subcutaneous fat and muscle. (Created with BioRender.com)

However, since the variations in these properties for individual layers are minimal, the resulting temperature variations are also insignificant. Their study shows that the small variations in physical parameters and variables have a negligible effect on the calculated temperature profiles. Especially the surface temperatures are strongly influenced by changes in the blood perfusion rate and the skin layer thickness [40].

1.3.1 Pennes' Bioheat Equation

The Pennes' bioheat Equation is the most commonly used form of heat transfer in soft, living tissue [49]. It provides a way to quantify the temperature distribution within tissues during thermal therapies or other situations involving heat transfer in living systems. The total energy exchange through the flowing blood is proportional to the volumetric heat flux and the temperature difference between the blood and the tissue [50]. The three-dimensional expression of Pennes' bioheat Equation for soft tissue with uniform material properties is given by Equation 1 [51]. This is a partial differential equation for the tissue temperature. With the correct initial conditions and boundary conditions, the transient and the steady-state temperature in the tissue can be determined [52].

$$\rho c \frac{dT}{dt} = k\frac{d^2T}{dx^2} + k\frac{d^2T}{dy^2} + k\frac{d^2T}{dz^2} + \omega_b c_b(T_a - T) + Q_m + Q_r(x,y,z,t)$$

Equation 1 - Pennes' bioheat Equation for human tissue in 3D (x,y,z direction)

The properties of the Pennes' bioheat Equation are as follows: T is the temperature in degree Celsius, ρ is tissue density [kg/m³], c is the specific heat of the tissue in [J/(kg K)], k is the tissue's thermal conductivity [W/(m K)], ω_b is the blood mass perfusion rate [kg/(m³s)] and c_b as blood specific heat [J/(kg K)]. The arterial temperature has the symbol T_a in degree Celsius, Q_m is the metabolic heat generation rate in [W/m³] and Q_r is the regional heat source [W/m³].

The Equation describes the balance between heat conduction, metabolic heat generation, and convective heat transfer through blood perfusion. The term Q_m accounts for the heat produced by cellular metabolic processes, while the term $\omega_b c_b(T_a - T)$ represents the heat exchange between the tissue and the blood flow. This term depends on the blood perfusion rate, blood specific heat capacity, and the temperature difference between the tissue and the arterial blood [53].

The two main mechanisms for heat flow within a tissue are conduction and convection. Conductive heat flow means that the temperature gradient within the tissue itself drives the flow. Convection of heat energy occurs through the blood that perfuses the tissue. Conductive heat flow is governed by Fourier's law of heat conduction. The law states (Equation 2) that the heat flux (q) through a material is directly proportional to the temperature gradient (dT/dx) across the material and its thermal conductivity (k). Mathematically, it can be expressed as:

$$q = -k\frac{dT}{dx}$$

Equation 2 - Fourier's law of thermal conduction

2. Materials and Methods

The objective of this proof-of-concept research is to enhance the methodology for utilizing dynamic infrared thermography (DIRT) in the assessment of both malignant and non-malignant skin lesions. In the future, the plan is to integrate various techniques such as dermoscopy, digital photography, hyperspectral imaging, and dynamic infrared thermography into an in-vivo measurement setup. To validate and assess the effectiveness of this new combined technique compared to existing clinical and diagnostic methods, large-scale clinical studies will be conducted. This proof of concept marks the initial phase of the research.

The investigation into the application of DIRT in skin cancer diagnostics is being carried out at the University of Antwerp, in collaboration with Ghent University Hospital and Antwerp University Hospital. The clinical trial has received approval from the ethical committee of the Antwerp University Hospital (BUN B3002022000057).

2.1 Data acquisition equipment

The data acquisition system comprises six primary components that are integrated into a measurement head to ensure consistent measurements. These components include a thermal camera, cooling device, RGB camera, laser diode, temperature and humidity sensor, and a computer for control and image processing.

The first component is a FLIR A700 long-wave infrared camera (7.5-14 µm) from Teledyne FLIR LLC, Oregon, USA. It utilizes an uncooled microbolometer detector with a pixel pitch of 12 µm and a thermal sensitivity (NETD) of <30 mK. Equipped with a 2.0x macro lens and a minimal focus distance of 18mm, the thermal camera captures 16-bit thermal image sequences at a resolution of 640 × 480 and a frame rate of 30 Hz. The thermal sequence is recorded in 16-bit RAW data at 30Hz. A two-point non-uniformity correction (NUC) is applied to the raw images using a blackbody as a reference at temperatures of 15 °C and 35 °C.

The second component is the Cryo 6 cold air unit from Zimmer MedizinSysteme GmbH, used as the cooling device for the skin lesion. This Class IIa medical device cools the skin in a non-contact, rapid, and reproducible manner without obstructing the field of view or interfering with the infrared camera [54]. The Cryo 6 generates filtered, moisture-free, oil-free, and quiet airflow at a temperature of -30 °C [55]. The airflow can be regulated in nine levels up to 1000l/min. Cooling is an optimal solution based on a literature review on skin cancer diagnosis with infrared thermography, ensuring uniform thermal excitation and high accuracy [23]. Non-contact cooling within the patient's physiological limitations is preferred for maintaining aseptic conditions.

A high-definition RGB endoscopic camera captures an RGB reference image before the thermal sequence begins. It also tracks and compensates for patient motion through post-processing and tracking algorithms. The endoscope operates at a frame rate of 30 fps with a resolution of 1280 × 720 pixels. It offers a 66° field of view and a depth of focus ranging from 3 to 8 cm. The combination of the endoscope and the infrared camera eliminates the need for a hyperthermic marker.

A laser dot diode emitting red light at a wavelength of 650 nm and light power below 5 mW is used to mark the center of the lesion. Monitoring the air flow near the skin lesion is facilitated by a Bosch BME280 sensor, which measures relative humidity, barometric pressure, and ambient temperature. The laser diode and the Bosch BME280 are controlled by an esp32 microcontroller using code developed by the authors.

A computer equipped with custom software controls the infrared camera, endoscope, laser dot diode, and cooling device. It also monitors the various sensors. All data is stored on the hard drive for further processing and analysis.

2.2 Acquisition protocol

Patient preparation is a crucial aspect that cannot be overlooked. To ensure accurate and reproducible thermal imaging, patient acclimatization should take place in a room with controlled temperature and humidity. Following a well-defined protocol is essential for maintaining consistency in the measurement procedure. A temperature-controlled environment is particularly important for clinical applications of thermal imaging. The examination room should maintain a sTable temperature within the range of 18 to 23 °C [56]. In this research, the examination room is set at a temperature of 22 °C. A calibrated sensor monitors both the temperature and humidity of the room. It is important to ensure that no airflow from the air conditioners is directed at the patient. If necessary, the patient removes appropriate clothing and jewelry. A minimum acclimatization time of 10 minutes is recommended to achieve sTable blood pressure and skin temperature.

The acquisition protocol commences with capturing a white light (RGB) image using a digital camera equipped with a macro lens. The measurement head, which integrates various components, is placed on the skin with the skin lesion positioned at the center of the measurement head. To protect the patient's skin, a foam ring with a thickness of 5 mm is attached to the measurement head. The laser mounted on the measurement head is used to mark the center of the lesion. The movement of the measurement head is recorded by the integrated endoscopic camera. The Flir A700 thermal camera is positioned 40 mm away from the skin lesion and incorporates an auto-focus feature to focus on the lesion. Initially, a 4-second sequence of steady-state infrared images is captured. This image sequence comprises 60 frames at a rate of 30 Hz. Following the recording of the steady-state images, the cooling

cycle is initiated. The parameters that can be easily adjusted include the air flow level and the duration of cooling. The Cryo cooling device is used to cool the skin area with a diameter of 50 mm, encompassing the lesion. Once the cooling load is removed, the thermal camera continues recording the natural reheating of both the skin lesion and the healthy surrounding skin for a duration of 1-5 minutes or until reaching a steady state.

2.3 Finite element skin model

Siemens NX is used to model the thermal FEM analysis. The geometry of the skin tissue for FEM analysis includes the shape of the model, number of layers, shape and size of the lesion. The model used in our preliminary research

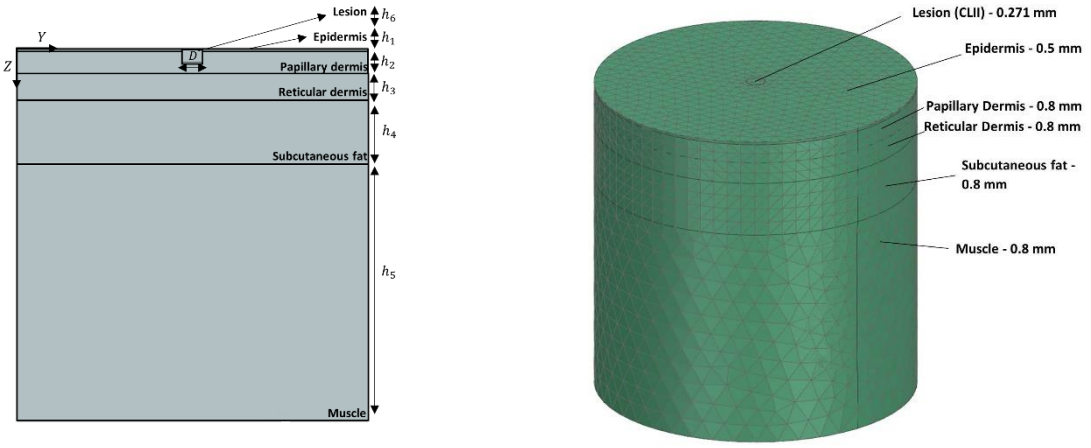

Figure 2 – (left) Layers of the skin in Siemens Simcenter 3D, (right) 3D cylindrical FEM model of human skin

is a three-dimensional cylindrical model with five skin layers as shown in Figure 2. This FEM model is implemented based on the research of Cëtingul and Herman [57]. A cylindrical 3D model is preferred over a 1D and 2D model as the latter two can lead to false or imprecise solutions and the cylindricity of the model requires less computational time due to only one lateral boundary condition on one face [58]. The five layers are the epidermis, papillary dermis, reticular dermis, subcutaneous fat and muscle. The size of the lesion is determined by the Clark level. The Clark Level is a staging system that describes the depth of the skin lesion as it grows.

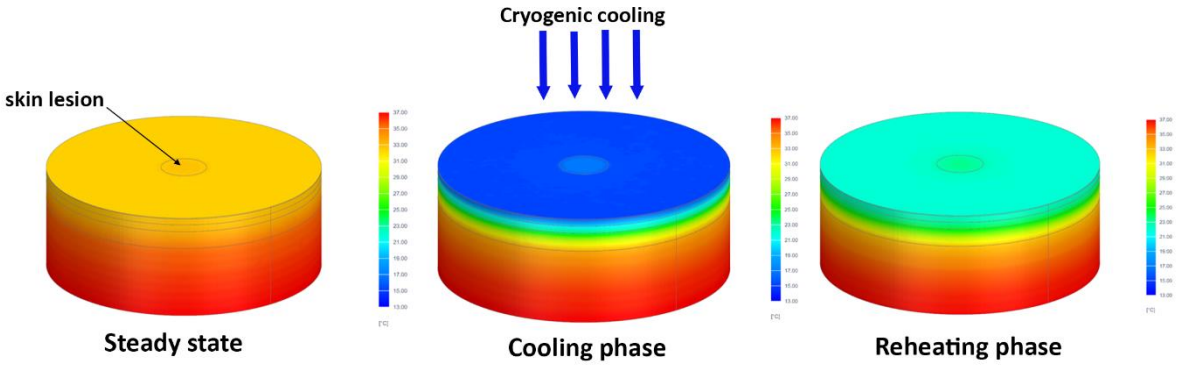

Figure 3 - Three phases of the skin model; from left to right, steady state phase, cooling phase and natural reheating phase

Table 1 gives an overview of the parameters used in this preliminary research. Properties of the skin layers are the height h_n, specific heat c_n, thermal conductivity k_n, density ρ_n, blood perfusion ω_b and metabolic heat generation Q_n. The parameters in Table 1 are from the study of Cetingül and Herman [40] based on values from literature. A 3D tetrahedral mesh type is chosen with different mesh sizes depending on the location of the mesh in the skin model. A finer mesh tends to be chosen for the most important regions for the determination of surface temperatures. The mesh sizes are shown in Figure 2.

The computational analysis consists of three phases, namely the steady-state phase, the cryogenic cooling phase and the reheating phase as shown in Figure 3. The steady state phase uses an ambient temperature of 21 °C, a blood temperature of 37 °C and a core body temperature of 37 °C. A convection heat transfer coefficient of 10 W/m²K is used, based on the properties of the ambient air. The last boundary condition is the tissue emissivity and has a value of ϵ = 0.98, determined and evaluated by Cheng and Herman [40], which can be considered as a constant value.

Layer	height h_n [mm]	specific Heat c_n $[\frac{J}{kgK}]$	thermal conductivity k_n $[\frac{W}{mK}]$	tissue density ρ_n $[\frac{kg}{m^3}]$	blood perfusion ω_b $[\frac{1}{s}]$	metabolic heat generation Q_n $[\frac{W}{m^3}]$
Epidermis [1]	0.1	3589	0.235	1200	0	0
Papillary Dermis [2]	0.7	3300	0.445	1200	0.0002	368.1
Reticular Dermis [3]	0.8	3300	0.445	1200	0.0013	368.1
Fat [4]	2	2674	0.185	1000	0.0001	368.3
Muscle [5]	8	3800	0.51	1085	0.0027	684.2
Lesion [6]	h_6= 0.2 - 1 D = 0.22 - 1.28	3852	0.558	1030	0.0063	3680

Table 1 - Nominal skin parameters used in this research according to Cetingül and Herman [37]

3. Results

3.1 In-Situ measurement head

The measurement head integrates the equipment mentioned in paragraph 2.1. It is specifically designed to allow the lesion to be cooled using the conditioned air from the Zimmer Cryo 6 cooler, while ensuring that the field of view of the macro lens remains unobstructed. Figure 4 illustrates the design of the measurement head, and the components utilized are described in section 2.1. Currently, the in-situ measurement head is undergoing thorough testing.

Preliminary results of the implemented imaging procedure can be observed in Figure 5. In its steady state, the lesion has a temperature of approximately 32 °C. Upon applying the cooling load for 60 seconds at flow level 9, the lesion's temperature decreased to around 4 °C. It should be noted that this cooling load exceeds what would be used in a clinical setting, but it is employed here to test the functionality of the in-situ measurement head. Additionally, the images display the rewarming frames at 20, 60, and 120 seconds. The skin lesion is clearly discernible in the infrared images.

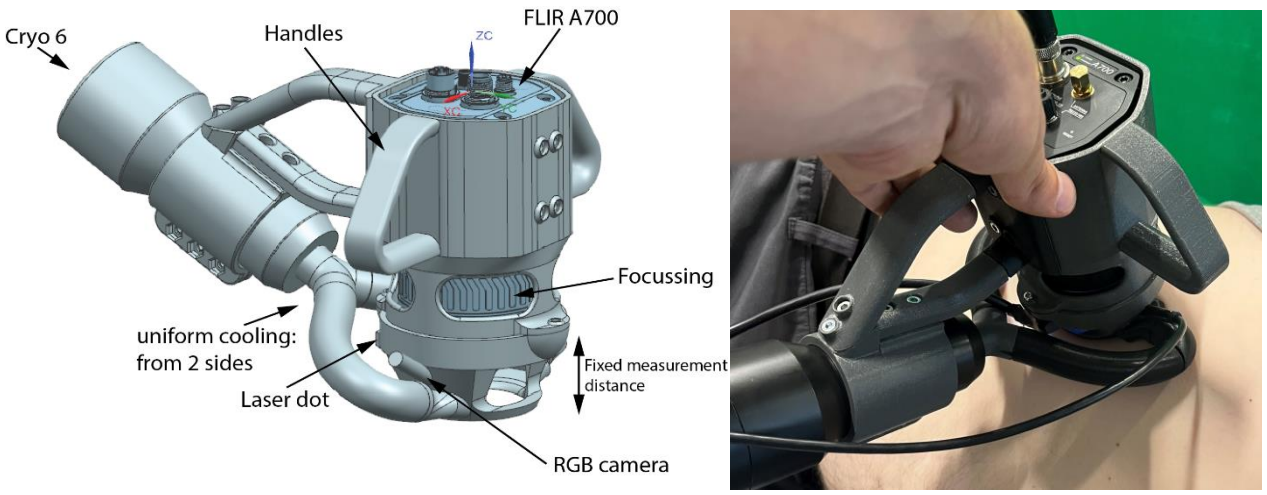

Figure 4 – (left) CAD model of the measurement head for DIRT on skin lesions, (right) in-situ measurement head during measurement

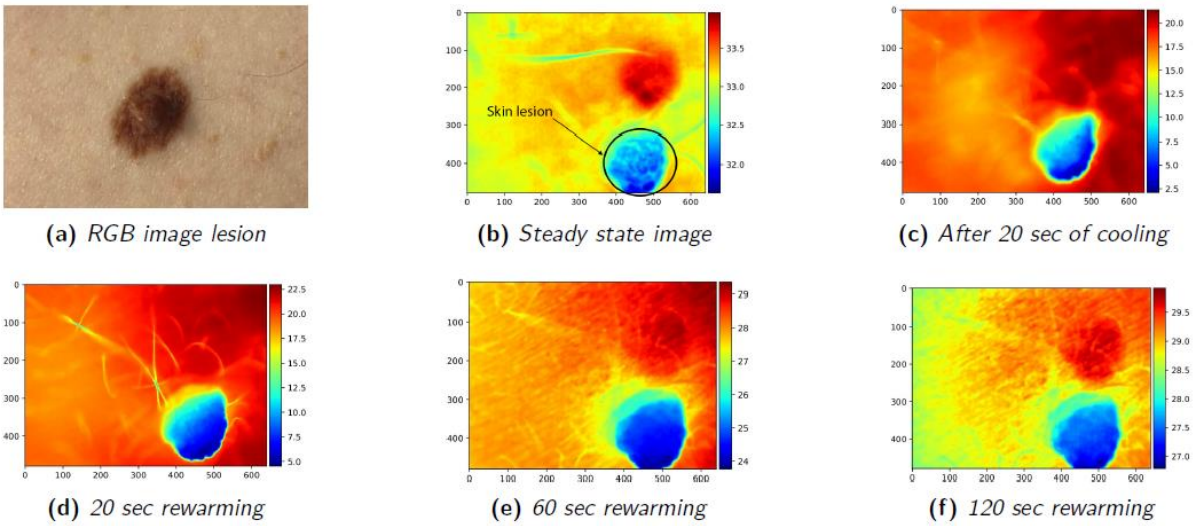

Figure 5 - RGB image and macro infrared thermography on skin lesion (20s of cooling, 120s rewarming)

3.2 Finite element skin model

Figure 6 presents the initial findings of the FEM skin model incorporating cryogenic cooling. Various cooling methods were simulated to determine the most suiTable approach for applying DIRT (Dynamic Infrared Thermography) for skin cancer diagnosis. The evaluated cooling methods included cryogenic cooling at two levels (level 1 and level 9), air cooling, constant cooling, and water cooling. Figure 7 illustrates the cooling effect of cryogenic cooling across different skin layers. Notably, the fat layer exhibits pronounced insulating properties.

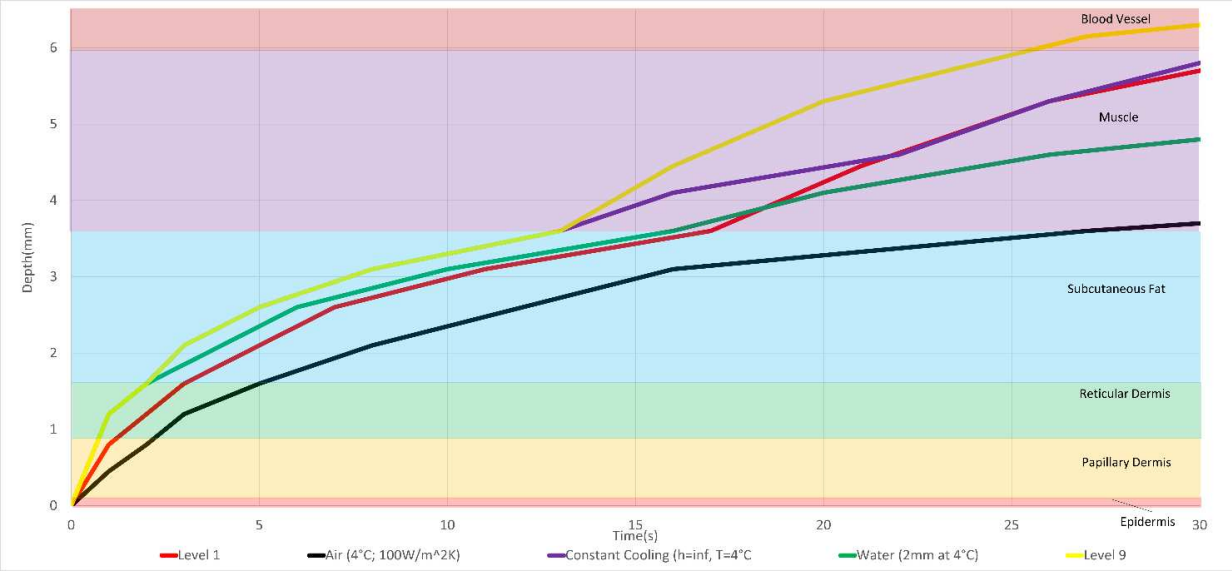

Figure 6 - Depth of cooling penetration into the skin for different cooling methods. The cryocooler is modelled at level 1 and level 9. Air cooling at 4°C, constant cooling and water cooling are included.

Two key observations emerge from the results. Firstly, higher flow levels of cryogenic cooling result in faster penetration through the skin layers. This observation holds true overall, with a particularly noTable difference between level 1 and level 9 (e.g., a 5-second disparity at the beginning of the muscle layer). Secondly, cooling at each flow level is virtually instantaneous above the epidermal layer, owing to the low thickness of the epidermis. Subsequently, as the cooling depth progresses from the start of the papillary dermis to the conclusion of the subcutaneous fat layer, the cooling rate gradually slows. This can be attributed to the varying thermal conductivity of the individual layers. Table 1 highlights the thermal conductivity disparities among the papillary dermis, reticular dermis, and subcutaneous fat layer. Specifically, the thermal conductivity of the papillary dermis and reticular dermis surpasses that of the subcutaneous fat layer. Consequently, layers with higher thermal conductivity experience faster heat transfer. Moreover, the cooling depth curve reaccelerates upon reaching the onset of the

muscle layer (i.e., the end of the subcutaneous fat layer) because the thermal conductivity of the muscle layer exceeds that of the subcutaneous fat layer.

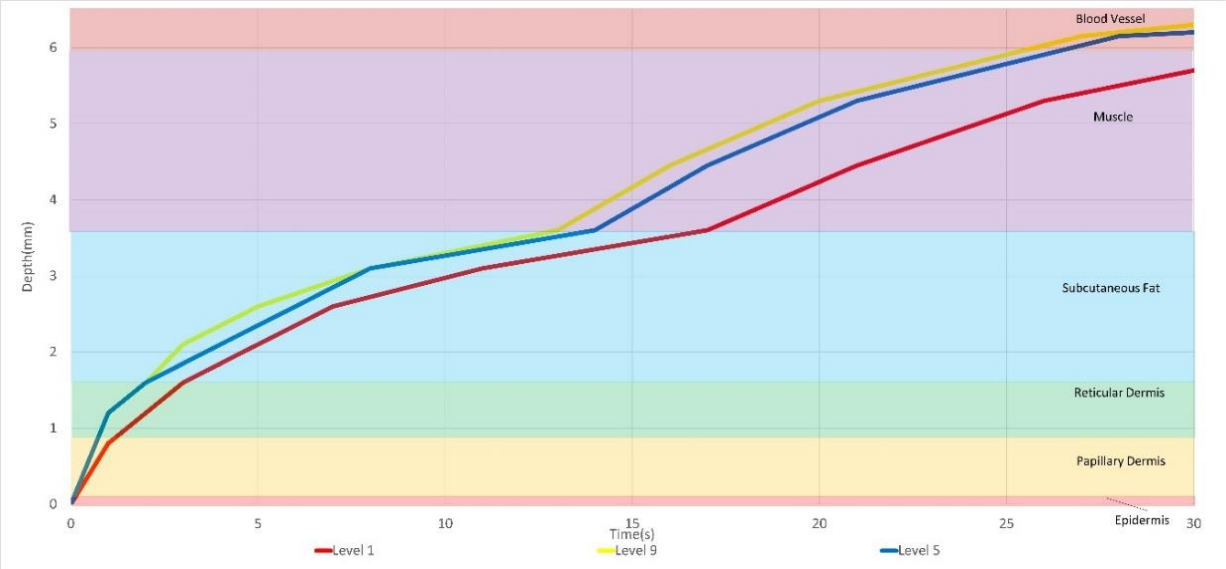

Figure 7 - Cooling depth in the skin layers in function of the time for cryogenic cooling at level 1,5 and 9

3.3 Clinical validation

In order to validate the Siemens Simcenter 3D thermal skin model, a preliminary study was conducted using a single pigmented lesion. The purpose of including only one lesion in this study was to facilitate the validation of the skin model. The lesion had a diameter of 15mm and displayed slight ulceration. The thermal response of both the skin lesion and healthy skin was measured using infrared imaging and compared with a model of the skin lesion created in Siemens Simcenter 3D. Figure 8 depicts an RGB color image of the pigmented lesion during the measurements, utilizing the measurement head described in section 3.1. The red laser dot indicates the center of the field of view for both the thermal and RGB cameras. The right image in the Figure illustrates the lesion in the thermal infrared spectrum, captured immediately after the cooling load was removed.

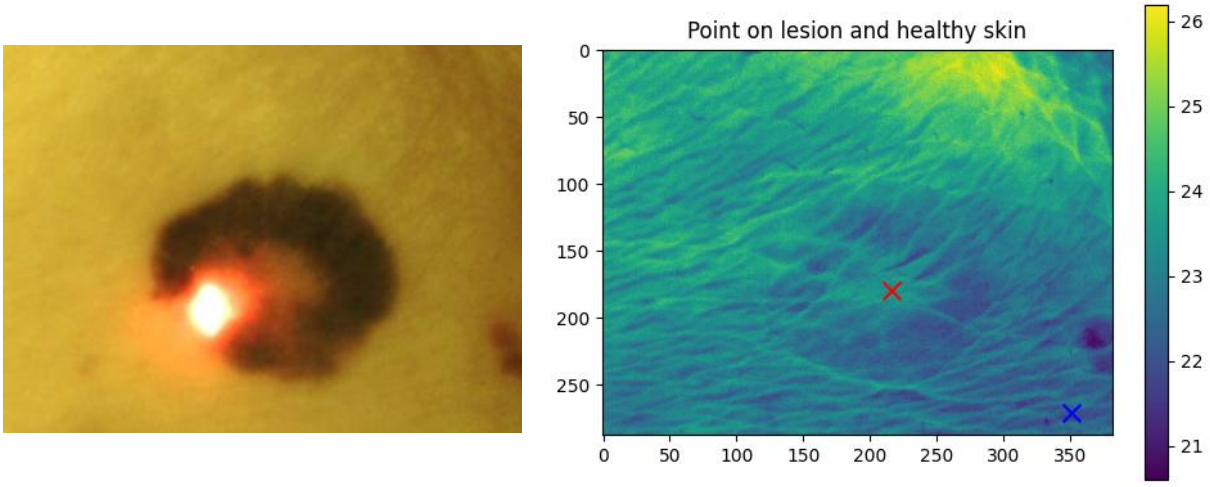

Figure 8 - (left) RGB image capturing the skin lesion, prominently displaying the red laser dot at its center, serving as a reference point within the field of view. (right) Red marker indicating the center of the lesion, while the blue marker represents the healthy skin region.

Upon applying the cooling load, the temperature of the lesion decreased to 28.59°C, while the temperature of the healthy skin was slightly lower at 27.15°C as can be seen in Figure 9. After approximately 60 seconds of reheating, the temperature of the lesion and healthy skin increased to around 33.09°C and 32.95°C, respectively. The temperature difference of more than 1°C between the lesion and healthy skin was clearly visible immediately after the cooling load was removed. However, this temperature difference gradually decreased as the reheating process continued. It should be noted that the magnitude and time evolution of this temperature difference varied based on the malignant potential of the lesion. The complete measurement cycle for the lesion and the healthy skin surrounding it is illustrated in Figure 10. The cycle begins with a 4-second steady state measurement, during which the center of the lesion exhibits a higher temperature compared to the surrounding healthy skin. Subsequently, both the lesion and healthy skin are cooled down for 20 seconds at flow level 7. It is observed that the lesion cools down to a lesser extent than the healthy skin during this cooling stage. Once the cooling load is removed, the process of reheating begins for both the lesion and healthy skin

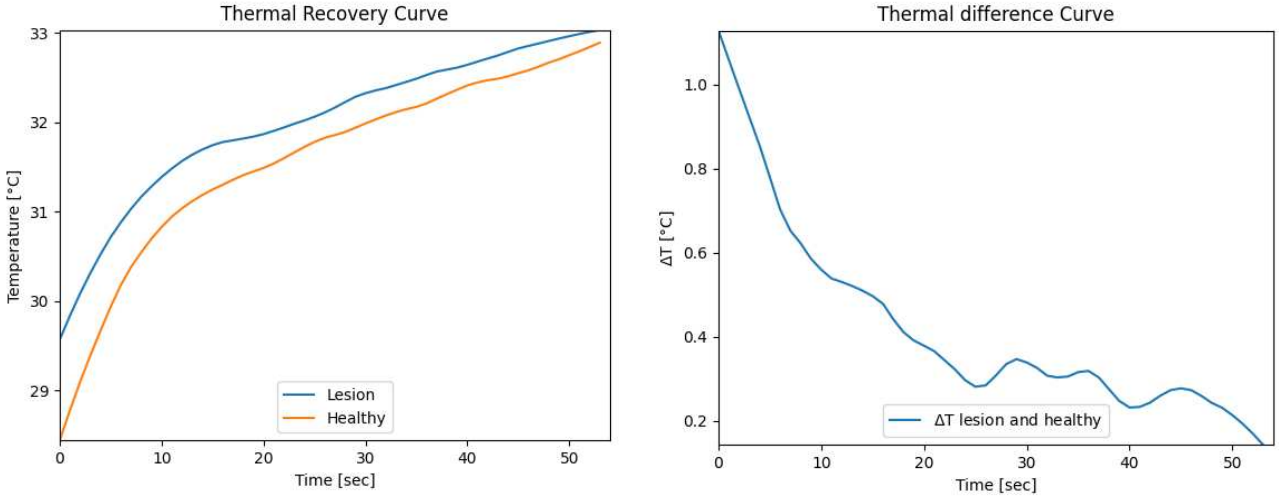

Figure 9 – (left) Time-dependent temperature profile of the pigmented lesion and healthy tissue. The lesion is denoted by the red cross, while the healthy skin is indicated by the blue cross, as shown in figure 8. (right) Thermal contrast between the lesion and healthy skin during the rewarming phase. A temperature difference exceeding 1 °C is immediately noticeable after the removal of the cooling load.

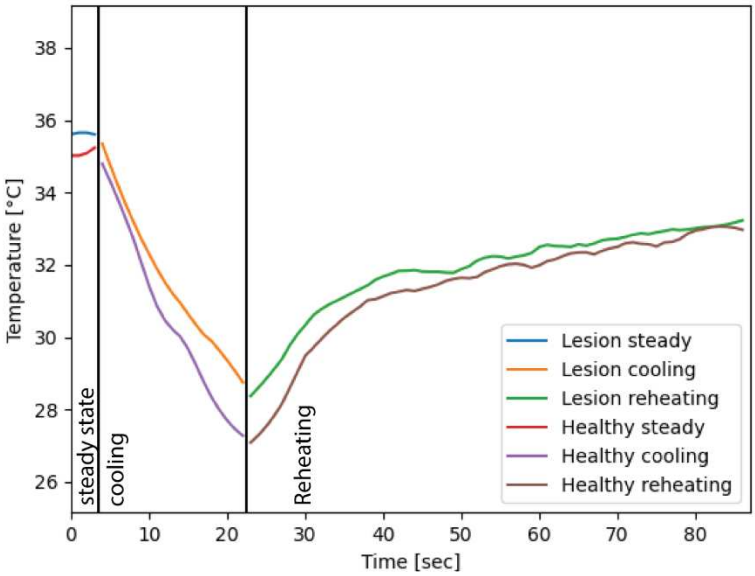

Figure 10 - Thermal curve depicting the steady state, cooling, and reheating sequences of the lesion (represented by the red cross in figure 8) and healthy skin (indicated by the blue cross in figure 8). Each sequence is captured consecutively with a slight delay, allowing for camera saving and restarting.

Input parameters for a thermal finite element model are vital in accurately simulating and predicting heat transfer behaviour within a system. These parameters include material properties such as thermal conductivity, specific heat capacity, and density, which define the thermal characteristics of the materials involved. The material parameters from Table 1 are used in this model. Geometric parameters, such as dimensions and boundary conditions, are essential for accurately representing the geometry and specifying the heat flow boundaries. The model has a diameter of 50 mm and a height of 11.8 mm. The lesion is modelled with a diameter of 15 mm and a height of 1 mm. The steady state model is shown in Figure 11: the center of the lesion and the healthy skin are depicted. Additional input parameters involve environmental factors, such as ambient temperature or radiation conditions, which can significantly influence the heat transfer process. Those parameters are listed in Table 2.

Parameter	Value	Unit
Steady state sequence	4	[seconds]
Cooling sequence	20	[seconds]
Reheating sequence	60	[seconds]
Ambient temperature	22	[°C]
Core body temperature	37	[°C]
Cryogenic cooling temperature	-30	[°C]
Air heat transfer Coefficient to room	2.5	$[W/m^2K]$
Emissivity	0.98	
Air speed at -30 °C	23.58	m/s

Table 2 – Parameters used as input for the FEM model in Siemens Simcenter 3D.

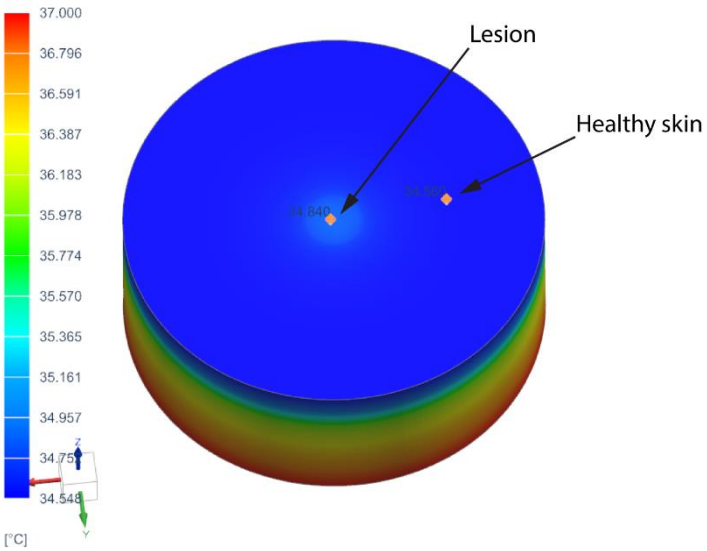

Figure 11 – Thermal model of the skin in steady state, featuring a central lesion (15mm diameter). The lesion registers a temperature of 34.84 °C, while the surrounding healthy skin exhibits a temperature of 34.56 °C.

Validating the accuracy and reliability of a thermal Finite Element Model (FEM) skin model through comparison with real data is crucial. This process involves examining the predicted thermal behaviour and temperature distribution of the FEM model and comparing it with experimental or measured data collected from real-world scenarios. In Figure 12, the thermal behaviour of the model is compared to the measurement data. Notably, during steady state, the temperature of the measured lesion and healthy skin surpasses that of the model. Throughout the cooling sequence, an interesting observation is that the model cools down at a faster rate than human skin, yet both reach the same temperature after 20 seconds of cooling. Additionally, the skin model exhibits a higher reheating rate compared to human skin, but ultimately reaches a nearly identical temperature after the 60-second mark.

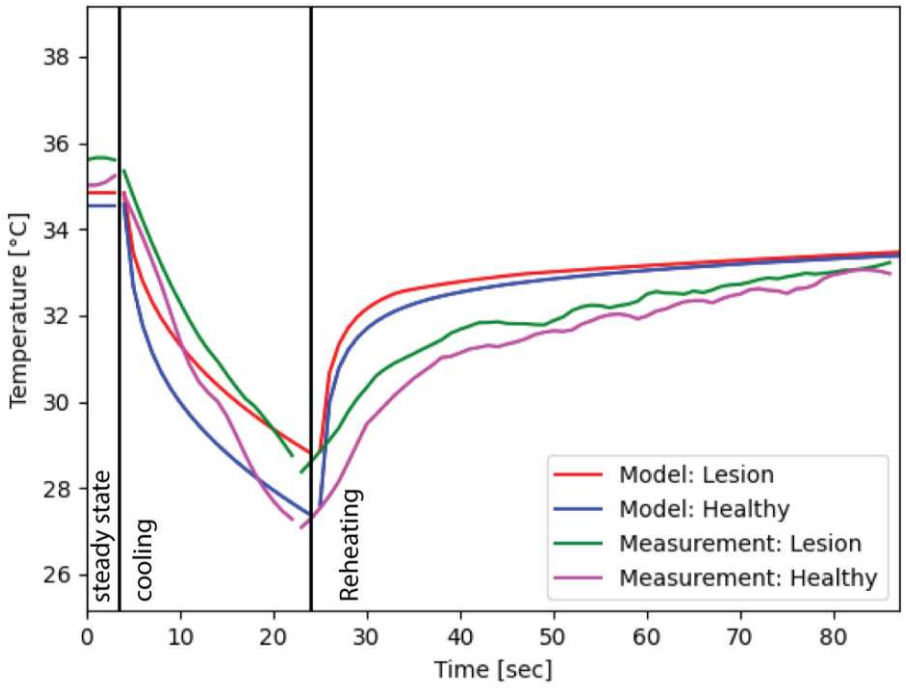

Figure 12 – Comparison of the thermal Finite Element Model (FEM) of the skin, using the parameters described in this paper, with thermal measurements on the pigmented skin lesion. Notably, the reheating rate of the model (shown in red and blue) differs from that of the pigmented lesion (depicted in green and magenta). The model exhibits overall behavior that aligns reasonably well with the measurements, although further enhancements, such as patient-specific models, could be implemented for improved accuracy.

4. Conclusion and Future work

In conclusion, skin cancer is a significant global health concern, with increasing incidence rates and a substantial impact on mortality. Early detection is crucial for improving survival rates and providing effective treatments. However, the current screening method of total body skin examination and subsequent biopsies has limitations, leading to unnecessary invasive procedures.

Dynamic infrared thermography (DIRT) has emerged as a potential non-invasive and quantitative technique for skin cancer diagnosis. By capturing thermal images and analyzing temperature variations, DIRT can detect differences in metabolic activity and angiogenesis associated with malignant skin lesions. The use of artificial intelligence and finite element models further enhances the accuracy and reliability of DIRT in diagnosing skin cancer.

A standardized measurement setup and protocol are essential for comparing measurements taken at different times. In this proof-of-concept research, a data acquisition system comprising a thermal camera, cooling device, RGB camera, laser diode, temperature and humidity sensor, and computer control was developed. The measurement hardware has undergone careful review and optimization to enhance measurement accuracy and repeatability. The system allows for consistent and accurate measurements during the DIRT procedure. Initial test measurements have yielded positive results, and the collected data is currently being processed. Although this

proof of concept for the measurement head has been successful, further adjustments to the instrument are still necessary to obtain optimal results.

When comparing the results of the finite element model and the measurements, the overall resemblance is knowledgeable. The model exhibits overall behavior that aligns reasonably well with the measurements, although further enhancements, such as patient-specific models, could be implemented for improved accuracy. The results of cooling the skin and cooling the model agree well, while there is still a difference in the heating of the real human skin and the model. Both in the model and in the measurements on the patient, a noticeable temperature difference is found between the healthy skin and the pigmented lesion. This indicates that the applied technique could possibly be used to distinguish between healthy and unhealthy skin.

By comparing various cooling techniques and durations, an optimal cooling protocol for thermal measurements of skin tissue can be identified in the future. In this work, the first steps are taken to build and validate a finite element skin model. While the basic finite element skin model in Siemens Simcenter 3D has not yet been thoroughly validated with real-life measurements, the initial findings and comparison demonstrates promising similarities to real-world scenarios. Since this study serves as a proof-of-concept, it is essential to clinically validate the cooling times. The FEM model provides an estimate of the minimum cooling time required to achieve sufficient cooling penetration. Furthermore, by making the model patient-specific, it becomes possible to customize the cooling times based on individual patients or specific anatomical locations.

Future research will focus on developing a system to mitigate uncontrolled movements of the measurement head and the patient. Additionally, efforts will be directed towards thermographic data processing, including motion tracking, image stabilization, image processing, segmentation, and lesion classification. The FEM skin model will be expanded and validated with more real-life measurements. The data generated by the FEM skin model will be used to train an AI network to be able to distinguish the healthy skin from the malign lesions.

Overall, the use of DIRT in skin cancer diagnosis shows promise in improving accuracy, reducing unnecessary biopsies, and providing a non-invasive and quantitative approach to assess malignant and non-malignant skin lesions. Further research and validation through extensive clinical studies are necessary to establish DIRT as a reliable and widely adopted tool in dermatology and skin cancer management.

Funding This research is funded by the Research Foundation-Flanders via support for the FWO research project, “Optimized skin tissue identification by combined thermal and hyperspectral imaging methodology.” (Project number 41882 (FWO G0A9720N) Jan Verstockt).

References

[1] H. Sung *et al.*, “Global Cancer Statistics 2020: GLOBOCAN Estimates of Incidence and Mortality Worldwide for 36 Cancers in 185 Countries,” *CA. Cancer J. Clin.*, vol. 71, no. 3, pp. 209–249, 2021, doi: 10.3322/caac.21660.

[2] WHO, “International Agency Research for Cancer, “Cancer WHOiafro. Estimated age-standardized incidence rates (World) in 2020, breast, woman, all ages.” http://gco.iarc.fr/today/home (accessed May 24, 2023).

[3] J. Verstockt, F. Thiessen, B. Cloostermans, W. Tjalma, and G. Steenackers, “DIEP flap breast reconstructions: thermographic assistance as a possibility for perforator mapping and improvement of DIEP flap quality,” *Appl. Opt.*, vol. 59, no. 17, p. E48, Jun. 2020, doi: 10.1364/AO.388351.

[4] M. M. Johnson *et al.*, “Skin cancer screening: recommendations for data-driven screening guidelines and a review of the US Preventive Services Task Force controversy,” *Melanoma Manag.*, vol. 4, no. 1, pp. 13–37, Mar. 2017, doi: 10.2217/mmt-2016-0022.

[5] S. G. Kandlikar *et al.*, “Infrared imaging technology for breast cancer detection – Current status, protocols and new directions,” *Int. J. Heat Mass Transf.*, vol. 108, pp. 2303–2320, May 2017, doi: 10.1016/j.ijheatmasstransfer.2017.01.086.

[6] A. Brunssen, A. Waldmann, N. Eisemann, and A. Katalinic, “Impact of skin cancer screening and secondary prevention campaigns on skin cancer incidence and mortality: A systematic review,” *J. Am. Acad. Dermatol.*, vol. 76, no. 1, pp. 129-139.e10, Jan. 2017, doi: 10.1016/j.jaad.2016.07.045.

[7] R. P. Braun, M. Oliviero, I. Kolm, L. E. French, A. A. Marghoob, and H. Rabinovitz, “Dermoscopy: what’s new?,” *Clin. Dermatol.*, vol. 27, no. 1, pp. 26–34, Jan. 2009, doi: 10.1016/j.clindermatol.2008.09.003.

[8] M. e. Vestergaard, P. Macaskill, P. e. Holt, and S. w. Menzies, “Dermoscopy compared with naked eye examination for the diagnosis of primary melanoma: a meta-analysis of studies performed in a clinical setting,” *Br. J. Dermatol.*, vol. 159, no. 3, pp. 669–676, 2008, doi: 10.1111/j.1365-2133.2008.08713.x.

[9] S. E. Godoy *et al.*, “Dynamic infrared imaging for skin cancer screening,” *Infrared Phys. Technol.*, vol. 70, pp. 147–152, May 2015, doi: 10.1016/j.infrared.2014.09.017.

[10] M. P. Çetingül and C. Herman, “Quantification of the thermal signature of a melanoma lesion,” *Int. J. Therm. Sci.*, vol. 50, no. 4, pp. 421–431, Apr. 2011, doi: 10.1016/j.ijthermalsci.2010.10.019.

[11] M. Bonmarin and F. A. Le Gal, “Chapter 31 - Thermal Imaging in Dermatology,” in *Imaging in Dermatology*, M. R. Hamblin, P. Avci, and G. K. Gupta, Eds., Boston: Academic Press, 2016, pp. 437–454. doi: 10.1016/B978-0-12-802838-4.00031-5.

[12] K. L. Williams, “Infrared Thermometry as a Tool in Medical Research,” *Ann. N. Y. Acad. Sci.*, vol. 121, no. 1, pp. 99–112, 1964, doi: 10.1111/j.1749-6632.1964.tb13689.x.
[13] B. F. Jones, “A reappraisal of the use of infrared thermal image analysis in medicine,” *IEEE Trans. Med. Imaging*, vol. 17, no. 6, pp. 1019–1027, Dec. 1998, doi: 10.1109/42.746635.
[14] A. Nowakowski and M. Kaczmarek, “Active Dynamic Thermography - Problems of implementation in medical diagnostics,” *Quant. InfraRed Thermogr. J.*, vol. 8, no. 1, pp. 89–106, Jun. 2011, doi: 10.3166/qirt.8.89-106.
[15] B. B. Lahiri, S. Bagavathiappan, T. Jayakumar, and J. Philip, “Medical applications of infrared thermography: A review,” *Infrared Phys. Technol.*, vol. 55, no. 4, pp. 221–235, Jul. 2012, doi: 10.1016/j.infrared.2012.03.007.
[16] F. E. F. Thiessen *et al.*, “Dynamic infrared thermography (DIRT) in Deep Inferior Epigastric Perforator (DIEP) flap breast reconstruction: standardization of the measurement set-up,” *Gland Surg.*, vol. 8, no. 6, pp. 799–805, Dec. 2019, doi: 10.21037/gs.2019.12.09.
[17] F. E. F. Thiessen *et al.*, “Dynamic Infrared Thermography (DIRT) in DIEP flap breast reconstruction: A clinical study with a standardized measurement setup,” *Eur. J. Obstet. Gynecol. Reprod. Biol.*, vol. 252, pp. 166–173, Sep. 2020, doi: 10.1016/j.ejogrb.2020.05.038.
[18] F. E. F. Thiessen *et al.*, “Dynamic Infrared Thermography (DIRT) in DIEP-flap breast reconstruction: A review of the literature,” *Eur. J. Obstet. Gynecol. Reprod. Biol.*, vol. 242, pp. 47–55, Nov. 2019, doi: 10.1016/j.ejogrb.2019.08.008.
[19] J. C. Torres-Galván, E. Guevara, E. S. Kolosovas-Machuca, A. Oceguera-Villanueva, J. L. Flores, and F. J. González, “Deep convolutional neural networks for classifying breast cancer using infrared thermography,” *Quant. InfraRed Thermogr. J.*, vol. 19, no. 4, pp. 283–294, Aug. 2022, doi: 10.1080/17686733.2021.1918514.
[20] M. Kaczmarek, A. Nowakowski, M. Suchowirski, J. Siebert, and W. Stojek, “Active dynamic thermography in cardiosurgery,” *Quant. InfraRed Thermogr. J.*, vol. 4, no. 1, pp. 107–123, Jun. 2007, doi: 10.3166/qirt.4.107-123.
[21] A. S. Hakim and R. N. Awale, “Extraction of hottest blood vessels from breast thermograms using state-of-the-art image segmentation methods,” *Quant. InfraRed Thermogr. J.*, vol. 19, no. 5, pp. 347–365, Oct. 2022, doi: 10.1080/17686733.2021.1974209.
[22] A. Özdil and B. Yılmaz, “Automatic body part and pose detection in medical infrared thermal images,” *Quant. InfraRed Thermogr. J.*, vol. 19, no. 4, pp. 223–238, Aug. 2022, doi: 10.1080/17686733.2021.1947595.
[23] J. Verstockt, S. Verspeek, F. Thiessen, W. A. Tjalma, L. Brochez, and G. Steenackers, “Skin Cancer Detection Using Infrared Thermography: Measurement Setup, Procedure and Equipment,” *Sensors*, vol. 22, no. 9, Art. no. 9, Jan. 2022, doi: 10.3390/s22093327.
[24] N. Akhter, R. Manza, S. Shaikh, B. Gawali, P. Yannawar, and S. Shaikh, “Diagnosis of Melanoma Using Thermography: A Review,” presented at the International Conference on Applications of Machine Intelligence and Data Analytics (ICAMIDA 2022), Atlantis Press, May 2023, pp. 466–473. doi: 10.2991/978-94-6463-136-4_40.
[25] C. Magalhaes, J. M. R. S. Tavares, J. Mendes, and R. Vardasca, “Comparison of machine learning strategies for infrared thermography of skin cancer,” *Biomed. Signal Process. Control*, vol. 69, p. 102872, Aug. 2021, doi: 10.1016/j.bspc.2021.102872.
[26] C. Magalhaes, J. Mendes, and R. Vardasca, “Meta-Analysis and Systematic Review of the Application of Machine Learning Classifiers in Biomedical Applications of Infrared Thermography,” *Appl. Sci.*, vol. 11, no. 2, Art. no. 2, Jan. 2021, doi: 10.3390/app11020842.
[27] C. Magalhaes, J. Mendes, and R. Vardasca, “The role of AI classifiers in skin cancer images,” *Skin Res. Technol.*, vol. 25, no. 5, pp. 750–757, 2019, doi: 10.1111/srt.12713.
[28] H. Chen, K. Wang, Z. Du, W. Liu, and Z. Liu, “Predicting the thermophysical properties of skin tumor based on the surface temperature and deep learning,” *Int. J. Heat Mass Transf.*, vol. 180, p. 121804, Dec. 2021, doi: 10.1016/j.ijheatmasstransfer.2021.121804.
[29] A. Kirimtat, O. Krejcar, and A. Selamat, “A Mini-review of Biomedical Infrared Thermography (B-IRT),” in *Bioinformatics and Biomedical Engineering*, I. Rojas, O. Valenzuela, F. Rojas, and F. Ortuño, Eds., in Lecture Notes in Computer Science, vol. 11466. Cham: Springer International Publishing, 2019, pp. 99–110. doi: 10.1007/978-3-030-17935-9_10.
[30] H. Qi and N. Diakides, “Infrared imaging in medicine,” University of Tennessee, 2007.
[31] Y. Y. Lee *et al.*, “Surrogate human sensor for human skin surface temperature measurement in evaluating the impacts of thermal behaviour at outdoor environment,” *Measurement*, vol. 118, pp. 61–72, Mar. 2018, doi: 10.1016/j.measurement.2018.01.010.
[32] W. Minkina and S. Dudzik, *Infrared Thermography - Errors and Uncertainties*, 1st ed. Wiley, 2009.
[33] T. M. Buzug, S. Schumann, L. Pfaffmann, U. Reinhold, and J. Ruhlmann, “Functional infrared imaging for skin-cancer screening,” in *Annual International Conference of the IEEE Engineering in Medicine and Biology - Proceedings*, 2006, pp. 2766–2769. doi: 10.1109/IEMBS.2006.259895.
[34] J. H. Flores-Sahagun, J. V. C. Vargas, and F. A. Mulinari-Brenner, “Analysis and diagnosis of basal cell carcinoma (BCC) via infrared imaging,” *Infrared Phys. Technol.*, vol. 54, no. 5, pp. 367–378, Sep. 2011, doi: 10.1016/j.infrared.2011.05.002.
[35] G. Santulli, *Angiogenesis: Insights from a Systematic Overview*. Nova Publisher, 2013.
[36] R. S. Kerbel, “Tumor Angiogenesis,” *N. Engl. J. Med.*, vol. 358, no. 19, pp. 2039–2049, May 2008, doi: 10.1056/NEJMra0706596.
[37] D. Elder, “Tumor Progression, Early Diagnosis and Prognosis of Melanoma,” *Acta Oncol.*, vol. 38, no. 5, pp. 535–548, Jan. 1999, doi: 10.1080/028418699431113.
[38] F. J. González, C. Castillo-Martínez, R. Valdes-Rodríguez, E. S. Kolosovas-Machuca, U. Villela-Segura, and B. Moncada, “Thermal signature of melanoma and non-melanoma skin cancers,” in *Proceedings of the 2012 International Conference on Quantitative InfraRed Thermography*, QIRT Council, 2012. doi: 10.21611/qirt.2012.276.

[39] L. J. Jiang *et al.*, “A perspective on medical infrared imaging,” *J. Med. Eng. Technol.*, vol. 29, no. 6, pp. 257–267, Jan. 2005, doi: 10.1080/03091900512331333158.
[40] M. P. Çetingül and C. Herman, “A heat transfer model of skin tissue for the detection of lesions: Sensitivity analysis,” *Phys. Med. Biol.*, vol. 55, no. 19, pp. 5933–5951, Oct. 2010, doi: 10.1088/0031-9155/55/19/020.
[41] D. A. Torvi and J. D. Dale, “A Finite Element Model of Skin Subjected to a Flash Fire,” *J. Biomech. Eng.*, vol. 116, no. 3, pp. 250–255, Aug. 1994, doi: 10.1115/1.2895727.
[42] M. P. Çetingül and C. Herman, “Transient Thermal Response of Skin Tissue,” presented at the ASME 2008 Heat Transfer Summer Conference collocated with the Fluids Engineering, Energy Sustainability, and 3rd Energy Nanotechnology Conferences, American Society of Mechanical Engineers Digital Collection, Jul. 2009, pp. 355–361. doi: 10.1115/HT2008-56409.
[43] P. Buliński, W. Adamczyk, and Z. Ostrowski, “Bioheat Transfer Model with Active Thermoregulation: Sensitivity of Temperature Field on Tissue Properties,” in *Innovations in Biomedical Engineering*, M. Gzik, E. Tkacz, Z. Paszenda, and E. Piętka, Eds., in Advances in Intelligent Systems and Computing. Cham: Springer International Publishing, 2017, pp. 259–266. doi: 10.1007/978-3-319-47154-9_30.
[44] Z. Ostrowski, P. Buliński, W. Adamczyk, P. Kozołub, and A. Nowak, “Numerical model of heat transfer in skin lesions,” *Sci. Lett. Univ. Rzesz. Technol. - Mech.*, vol. 32, no. 87(1/2015), pp. 55–62, 2015, doi: 10.7862/rm.2015.6.
[45] S. K. Kandala, D. Deng, and C. Herman, “Simulation of Discrete Blood Vessel Effects on the Thermal Signature of a Melanoma Lesion,” in *Volume 3B: Biomedical and Biotechnology Engineering*, San Diego, California, USA: American Society of Mechanical Engineers, Nov. 2013, p. V03BT03A038. doi: 10.1115/IMECE2013-64451.
[46] P. Wongchadakul and P. Rattanadecho, “Mathematical Modeling of Multilayered Skin with Embedded Tumor Through Combining Laser Ablation and Nanoparticles: Effects of Laser Beam Area, Wavelength, Intensity, Tumor Absorption Coefficient and Its Position,” *Int. J. Heat Technol.*, vol. 39, no. 1, pp. 89–100, Feb. 2021, doi: 10.18280/ijht.390109.
[47] M. Strąkowska and B. Więcek, “Thermal modeling of planar and cylindrical biomedical multilayers structures in frequency domain,” *Meas. Autom. Monit.*, no. Vol. 65, No. 2, pp. 32--36, 2019.
[48] T. C. Barros and A. A. A. Figueiredo, “Three-dimensional numerical evaluation of skin surface thermal contrast by application of hypothermia at different depths and sizes of the breast tumor,” *Comput. Methods Programs Biomed.*, vol. 236, p. 107562, Jun. 2023, doi: 10.1016/j.cmpb.2023.107562.
[49] C. Hildebrandt, C. Raschner, and K. Ammer, “An Overview of Recent Application of Medical Infrared Thermography in Sports Medicine in Austria,” *Sensors*, vol. 10, no. 5, Art. no. 5, May 2010, doi: 10.3390/s100504700.
[50] W. Shen, J. Zhang, and F. Yang, “Modeling and numerical simulation of bioheat transfer and biomechanics in soft tissue,” *Math. Comput. Model.*, vol. 41, no. 11–12, pp. 1251–1265, May 2005, doi: 10.1016/j.mcm.2004.09.006.
[51] H. H. Pennes, “Analysis of tissue and arterial blood temperatures in the resting human forearm. 1948.,” *J. Appl. Physiol.*, 1948, doi: 10.1152/JAPPL.1948.1.2.93.
[52] L. Zhu, “Chapter 2 Heat Transfer applications in Biological Systems,” *McGraw-Hill Educ.*, vol. Volume 1, no. Biomedical Engineering and Design Handbook, 2010, Accessed: May 19, 2022. [Online]. Available: https://www.semanticscholar.org/paper/CHAPTER-2-HEAT-TRANSFER-APPLICATIONS-IN-BIOLOGICAL-Zhu/a56e3ec383e867de9956eac63f00645c39356047
[53] N. Sarkar, “A novel Pennes’ bioheat transfer equation with memory-dependent derivative,” *Math. Models Eng.*, vol. 2, no. 2, pp. 151–157, Dec. 2016, doi: 10.21595/mme.2016.18024.
[54] “MDCG 2021-24 - Guidance on classification of medical devices.” https://ec.europa.eu/health/latest-updates/mdcg-2021-24-guidance-classification-medical-devices-2021-10-04_en (accessed May 11, 2022).
[55] “Cryo 6 Brochure - Information About the Zimmer Skin Cooling Chiller,” *Zimmer MedizinSystems*. https://zimmerusa.com/products/cryo-therapy/cryo-6/cryo-6-brochure/ (accessed May 11, 2022).
[56] R. Vardasca, L. Vaz, and J. Mendes, “Classification and Decision Making of Medical Infrared Thermal Images,” in *Classification in BioApps*, N. Dey, A. S. Ashour, and S. Borra, Eds., in Lecture Notes in Computational Vision and Biomechanics, vol. 26. Cham: Springer International Publishing, 2018, pp. 79–104. doi: 10.1007/978-3-319-65981-7_4.
[57] M. P. Çetingül and C. Herman, “A heat transfer model of skin tissue for the detection of lesions: sensitivity analysis,” *Phys. Med. Biol.*, vol. 55, no. 19, pp. 5933–5951, Sep. 2010, doi: 10.1088/0031-9155/55/19/020.
[58] J. Iljaž, L. C. Wrobel, M. Hriberšek, and J. Marn, “Numerical modelling of skin tumour tissue with temperature-dependent properties for dynamic thermography,” *Comput. Biol. Med.*, vol. 112, p. 103367, Sep. 2019, doi: 10.1016/j.compbiomed.2019.103367.

Finite element skin models as additional data for dynamic infrared thermography on skin lesions

by Jan Verstockt[*], Ruben Somers[*], Filip Thiessen[**], Isabelle Hoorens[***], Lieve Brochez[***], Gunther Steenackers[*]

[*] *InViLab Research Group, University of Antwerp, Groenenborgerlaan 171, B-2020 Antwerp, Belgium*
[**] *Department of Plastic, Reconstructive and Aesthetic Surgery, Multidisciplinary Breast Clinic, Antwerp University Hospital, University of Antwerp, Wilrijkstraat 10, B-2650 Antwerp, Belgium*
[***] *Department of Dermatology, Ghent University Hospital, C. Heymanslaan 10, B-9000 Ghent, Belgium*

Abstract

Skin cancer is a significant global health concern, with increasing incidence rates and a high number of deaths each year. Early detection plays a crucial role in improving survival rates, but current screening methods, such as total body skin examination, often lead to unnecessary invasive excisions. This research aims to explore the use of dynamic infrared thermography (DIRT) in combination with other technologies to potentially eliminate the need for biopsies in the future and gather information about the stage or depth of malignant skin lesions. This article focuses on using DIRT in skin cancer diagnostics and presents a proof-of-concept study conducted at the University of Antwerp (Belgium). The study involves data acquisition using a thermal camera and a finite element skin model. The FEM skin model employed in this research follows the commonly used five-layer model. Each layer is assigned specific thermophysical properties such as thermal conductivity, blood perfusion rate, and thickness. A FEM skin model in Siemens Simcenter 3D is constructed to be able to simulate the cryogenic cooling on the skin. It is possible to improve the thermal images by choosing an appropriate cooling method, cooling sequence and optimized measurement setup. While the FEM skin model shares certain similarities with the measurement data, there is room for further enhancements to optimize its performance. The acquired data is analyzed to assess the effectiveness of the combined technique compared to existing clinical and diagnostic methods.

Keywords: Finite element model, skin cancer, dynamic infrared thermography, data augmentation, FEM, Pennes

1. Introduction

1.1 Skin Cancer

Cancer is a significant global health concern, with an estimated annual toll of almost 10 million deaths and more than 19 million new cases worldwide [1]. The incidence rates of melanoma, a type of skin cancer, have tripled in Europe and the United States over the past four decades [1], [2]. Nonmelanoma skin cancer, contributes to over one million new cases (1,198,073 or 11% of estimated new cases in 2020, worldwide for both sexes and all ages) and 64,000 (0.6%) deaths each year globally. Men are affected at a rate twice as high as women. Melanoma skin cancer accounts for more than 324,635 (3.4% of estimated new cases in 2020, worldwide for both sexes and all ages) new cases and approximately 60,000 (0.6%) deaths annually [1].

Skin cancer encompasses various pathological conditions arising from different cell types in the epidermis and dermis. It is primarily categorized into melanoma and non-melanoma skin cancer, with the latter mainly comprising keratinocyte cancers (basal and squamous cell carcinomas) and rarer types like Merkel cell carcinoma[1], [2]. Early detection plays a crucial role in improving survival rates and enabling more effective and cost-efficient treatments with minimal impact on patients' quality of life [3]. Regular screening is recommended for specific high-risk populations, such as annual breast cancer screening for older women and annual lung cancer screening for individuals aged 55 to 74 with a history of smoking [4], [5]. Presently, a total body skin examination (TBSE) is the commonly used screening method [4]. Dermatologists perform this inexpensive and non-invasive procedure to identify potential malignant and benign skin lesions. The accuracy of their diagnoses is influenced by their training and experience [6]. Trained dermatologists can enhance accuracy by incorporating polarized light dermoscopy, which highlights additional features like pigmentation or vascularization [7], [8]. However, invasive excisions are still conducted to rule out false-negative findings that could lead to metastasis and death. Unfortunately, many of these excisions are unnecessary, as only one melanoma is detected for every 10 to 60 biopsies performed [9], [10].

The purpose of this research is to explore the use of dynamic infrared thermography, in combination with technologies such as finite element (FEM) models of the human skin, digital dermoscopy and hyperspectral imaging (the latter two are not in the scope of this article), to potentially eliminate the need for biopsies in the future. Additionally in future work, the aim is to gather information about the stage or depth of malignant skin lesions. This information can assist surgeons in accurately removing the malignant skin lesion by detecting the subcutaneous area.

1.2 Dynamic infrared thermography in biomedical applications

The use of infrared thermal imaging in biomedical applications was uncommon in the past. The bulky first-generation IR cameras and their limited performance together with the unsatisfactory results of passive thermography are the root cause [11]–[13] . Active dynamic thermography and the problems to implement it in medical diagnostics has been extensively discussed by Nowakowski et al. [14]. Infrared thermography has been continuously improved over the last years and is recently widely used in biomedical applications for the detection of breast cancer, psoriasis, fever screening, dentistry or measuring flap perfusion during breast reconstruction with DIEP flaps [15]–[19] or even in cardiosurgery and the detection of blood vessels [20], [21]. Also body part and pose estimation based on medical thermographic images has been researched[22]. A full review on infrared thermography on skin cancer is out of the scope of this article but can be found in previous contributions [23], [24].

Recent additions to literature on the detection of cancers with infrared thermography are mostly based on a combination of artificial intelligence (AI) and numerical models with infrared thermography. Magalhaes et al. conducted research on the role of different AI classifiers in skin cancers images, not only limited to infrared thermography [25]. In the following work they did a comparison of the application of machine learning strategies for infrared thermography of skin cancer [26], [27]. Chen et al. trained an AI model on data generated by a 3D FEM model to extract the thermophysical properties of the skin cancer [28].

1.2.1 Skin cancer diagnosis using thermography – working principle

Biomedical infrared thermography reveals the heterogeneous skin and superficial tissue temperature [29]. Infrared emissions from human skin at 27 °C are in the wavelength range of 2–20 μm , and peaks at 10 μm. The term body infrared rays, a narrow wavelength range of 8–12 μm, is used for medical applications [30]. As reported by Lee and Minkina, the commonly accepted emissivity ϵ of human skin, independent of the skin pigmentation, is 0.98 ± 0.01 for $\lambda > 2$ μm, which makes human skin a close to perfect black body [13], [31]–[33].

As a living organism, the human body attempts to maintain homeostasis, the balance of all systems in the body, for all physiological processes, resulting in dynamic changes in heat output [3]. The result of a complicated combination of central and local regulatory systems is reflected in the surface temperature of an extremity. Core body temperature is maintained constant at depths greater than 20 mm [33]. Skin surface temperature is a useful indicator of health problems or physical disorders of skin-related processes [33]. Skin cancer cells are different compared to normal skin cells due to the high rate of uncontrolled cell division [34]. As a result of the high rate of cell division, cancer cells need to convert more energy to support the cellular processes. Due to the high metabolic rate, there is a higher energy demand, which also leads to increased angiogenesis. Angiogenesis is the physiological process by which new blood vessels form from existing vessels to provide the necessary additional energy [35], [36]. In conjunction with the increased energy requirements, melanoma skin lesions are thought to have a higher temperature (Δ 2–4 K) than the surrounding healthy skin [33], [37], [38].The IR imaging of melanoma skin lesions is based on the detection of new blood vessels and chemical changes associated with a tumour development and growth [39]. Currently, there is no standardized, reliable, quantitative, and non-invasive method based on IRT to accurately determine the malignant potential of skin lesions [10].

1.3 Finite element skin model

IR imaging combined with a mathematical model is used to understand the temporal evolution and time constants of the process [40]. This is a challenging task due to the many parameters of the Pennes's bioheat Equation (see section 1.3.1). Not only differ the thermophysical parameters from patient to patient but also the dimensions and position of the lesions, as well as the lesion parameters are patient dependant [41]. The Pennes bioheat Equation is not only used to study cancers of the skin [42]–[47] but also for simulating breast tumor analysis [28], [48]. The five-layer model is most commonly used to determine the temperature distribution during cooling. This model consists of the epidermis, papillary dermis, reticular dermis, subcutaneous fat and muscle. The FEM model implements the Pennes bioheat Equation. The parameters of the five layers used in the Pennes' bioheat Equation are shown in Table 1 and Table 2. With a mathematical model, the excitation method (cooling of the skin) can be analysed. The model can be used to conduct a parameter sensitivity study to gain understanding of the human skin

system. Cëtingul and Herman discovered that the thermal response of a lesion is mainly influenced by its total volume, average equivalent diameter, and penetration depth (stage), while small protrusions and irregularities have a relatively minor effect [40]. Cëtingul and Herman evaluated the effects of variations in thermophysical properties, metabolic heat generation, blood perfusion rate, and skin layer thickness on the distribution of surface temperatures, skin layers are tested and subjected to cooling and subsequent thermal recovery.

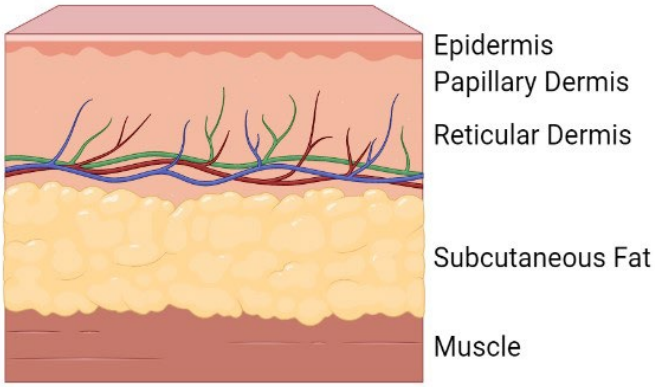

Figure 1- The 5-layer skin model consists of the epidermis, papillary dermis, reticular dermis, subcutaneous fat and muscle. (Created with BioRender.com)

However, since the variations in these properties for individual layers are minimal, the resulting temperature variations are also insignificant. Their study shows that the small variations in physical parameters and variables have a negligible effect on the calculated temperature profiles. Especially the surface temperatures are strongly influenced by changes in the blood perfusion rate and the skin layer thickness [40].

1.3.1 Pennes' Bioheat Equation

The Pennes' bioheat Equation is the most commonly used form of heat transfer in soft, living tissue [49]. It provides a way to quantify the temperature distribution within tissues during thermal therapies or other situations involving heat transfer in living systems. The total energy exchange through the flowing blood is proportional to the volumetric heat flux and the temperature difference between the blood and the tissue [50]. The three-dimensional expression of Pennes' bioheat Equation for soft tissue with uniform material properties is given by Equation 1 [51]. This is a partial differential equation for the tissue temperature. With the correct initial conditions and boundary conditions, the transient and the steady-state temperature in the tissue can be determined [52].

$$\rho c \frac{dT}{dt} = k\frac{d^2T}{dx^2} + k\frac{d^2T}{dy^2} + k\frac{d^2T}{dz^2} + \omega_b c_b (T_a - T) + Q_m + Q_r(x,y,z,t)$$

Equation 1 - Pennes' bioheat Equation for human tissue in 3D (x,y,z direction)

The properties of the Pennes' bioheat Equation are as follows: T is the temperature in degree Celsius, ρ is tissue density [kg/m³], c is the specific heat of the tissue in [J/(kg K)], k is the tissue's thermal conductivity [W/(m K)], ω_b is the blood mass perfusion rate [kg/(m³s)] and c_b as blood specific heat [J/(kg K)]. The arterial temperature has the symbol T_a in degree Celsius, Q_m is the metabolic heat generation rate in [W/m³] and Q_r is the regional heat source [W/m³].

The Equation describes the balance between heat conduction, metabolic heat generation, and convective heat transfer through blood perfusion. The term Q_m accounts for the heat produced by cellular metabolic processes, while the term $\omega_b c_b (T_a - T)$ represents the heat exchange between the tissue and the blood flow. This term depends on the blood perfusion rate, blood specific heat capacity, and the temperature difference between the tissue and the arterial blood [53].

The two main mechanisms for heat flow within a tissue are conduction and convection. Conductive heat flow means that the temperature gradient within the tissue itself drives the flow. Convection of heat energy occurs through the blood that perfuses the tissue. Conductive heat flow is governed by Fourier's law of heat conduction. The law states (Equation 2) that the heat flux (q) through a material is directly proportional to the temperature gradient (dT/dx) across the material and its thermal conductivity (k). Mathematically, it can be expressed as:

$$q = -k\frac{dT}{dx}$$

Equation 2 - Fourier's law of thermal conduction

2. Materials and Methods

The objective of this proof-of-concept research is to enhance the methodology for utilizing dynamic infrared thermography (DIRT) in the assessment of both malignant and non-malignant skin lesions. In the future, the plan is to integrate various techniques such as dermoscopy, digital photography, hyperspectral imaging, and dynamic infrared thermography into an in-vivo measurement setup. To validate and assess the effectiveness of this new combined technique compared to existing clinical and diagnostic methods, large-scale clinical studies will be conducted. This proof of concept marks the initial phase of the research.

The investigation into the application of DIRT in skin cancer diagnostics is being carried out at the University of Antwerp, in collaboration with Ghent University Hospital and Antwerp University Hospital. The clinical trial has received approval from the ethical committee of the Antwerp University Hospital (BUN B3002022000057).

2.1 Data acquisition equipment

The data acquisition system comprises six primary components that are integrated into a measurement head to ensure consistent measurements. These components include a thermal camera, cooling device, RGB camera, laser diode, temperature and humidity sensor, and a computer for control and image processing.

The first component is a FLIR A700 long-wave infrared camera (7.5-14 µm) from Teledyne FLIR LLC, Oregon, USA. It utilizes an uncooled microbolometer detector with a pixel pitch of 12 µm and a thermal sensitivity (NETD) of <30 mK. Equipped with a 2.0x macro lens and a minimal focus distance of 18mm, the thermal camera captures 16-bit thermal image sequences at a resolution of 640 × 480 and a frame rate of 30 Hz. The thermal sequence is recorded in 16-bit RAW data at 30Hz. A two-point non-uniformity correction (NUC) is applied to the raw images using a blackbody as a reference at temperatures of 15 °C and 35 °C.

The second component is the Cryo 6 cold air unit from Zimmer MedizinSysteme GmbH, used as the cooling device for the skin lesion. This Class IIa medical device cools the skin in a non-contact, rapid, and reproducible manner without obstructing the field of view or interfering with the infrared camera [54]. The Cryo 6 generates filtered, moisture-free, oil-free, and quiet airflow at a temperature of -30 °C [55]. The airflow can be regulated in nine levels up to 1000l/min. Cooling is an optimal solution based on a literature review on skin cancer diagnosis with infrared thermography, ensuring uniform thermal excitation and high accuracy [23]. Non-contact cooling within the patient's physiological limitations is preferred for maintaining aseptic conditions.

A high-definition RGB endoscopic camera captures an RGB reference image before the thermal sequence begins. It also tracks and compensates for patient motion through post-processing and tracking algorithms. The endoscope operates at a frame rate of 30 fps with a resolution of 1280 × 720 pixels. It offers a 66° field of view and a depth of focus ranging from 3 to 8 cm. The combination of the endoscope and the infrared camera eliminates the need for a hyperthermic marker.

A laser dot diode emitting red light at a wavelength of 650 nm and light power below 5 mW is used to mark the center of the lesion. Monitoring the air flow near the skin lesion is facilitated by a Bosch BME280 sensor, which measures relative humidity, barometric pressure, and ambient temperature. The laser diode and the Bosch BME280 are controlled by an esp32 microcontroller using code developed by the authors.

A computer equipped with custom software controls the infrared camera, endoscope, laser dot diode, and cooling device. It also monitors the various sensors. All data is stored on the hard drive for further processing and analysis.

2.2 Acquisition protocol

Patient preparation is a crucial aspect that cannot be overlooked. To ensure accurate and reproducible thermal imaging, patient acclimatization should take place in a room with controlled temperature and humidity. Following a well-defined protocol is essential for maintaining consistency in the measurement procedure. A temperature-controlled environment is particularly important for clinical applications of thermal imaging. The examination room should maintain a sTable temperature within the range of 18 to 23 °C [56]. In this research, the examination room is set at a temperature of 22 °C. A calibrated sensor monitors both the temperature and humidity of the room. It is important to ensure that no airflow from the air conditioners is directed at the patient. If necessary, the patient removes appropriate clothing and jewelry. A minimum acclimatization time of 10 minutes is recommended to achieve sTable blood pressure and skin temperature.

The acquisition protocol commences with capturing a white light (RGB) image using a digital camera equipped with a macro lens. The measurement head, which integrates various components, is placed on the skin with the skin lesion positioned at the center of the measurement head. To protect the patient's skin, a foam ring with a thickness of 5 mm is attached to the measurement head. The laser mounted on the measurement head is used to mark the center of the lesion. The movement of the measurement head is recorded by the integrated endoscopic camera. The Flir A700 thermal camera is positioned 40 mm away from the skin lesion and incorporates an auto-focus feature to focus on the lesion. Initially, a 4-second sequence of steady-state infrared images is captured. This image sequence comprises 60 frames at a rate of 30 Hz. Following the recording of the steady-state images, the cooling

cycle is initiated. The parameters that can be easily adjusted include the air flow level and the duration of cooling. The Cryo cooling device is used to cool the skin area with a diameter of 50 mm, encompassing the lesion. Once the cooling load is removed, the thermal camera continues recording the natural reheating of both the skin lesion and the healthy surrounding skin for a duration of 1-5 minutes or until reaching a steady state.

2.3 Finite element skin model

Siemens NX is used to model the thermal FEM analysis. The geometry of the skin tissue for FEM analysis includes the shape of the model, number of layers, shape and size of the lesion. The model used in our preliminary research

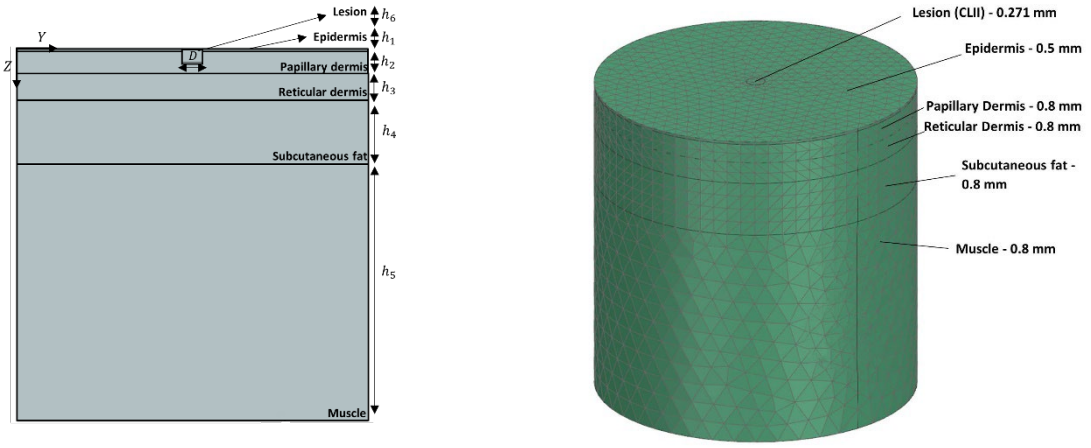

Figure 2 – (left) Layers of the skin in Siemens Simcenter 3D, (right) 3D cylindrical FEM model of human skin

is a three-dimensional cylindrical model with five skin layers as shown in Figure 2. This FEM model is implemented based on the research of Cëtingul and Herman [57]. A cylindrical 3D model is preferred over a 1D and 2D model as the latter two can lead to false or imprecise solutions and the cylindricity of the model requires less computational time due to only one lateral boundary condition on one face [58]. The five layers are the epidermis, papillary dermis, reticular dermis, subcutaneous fat and muscle. The size of the lesion is determined by the Clark level. The Clark Level is a staging system that describes the depth of the skin lesion as it grows.

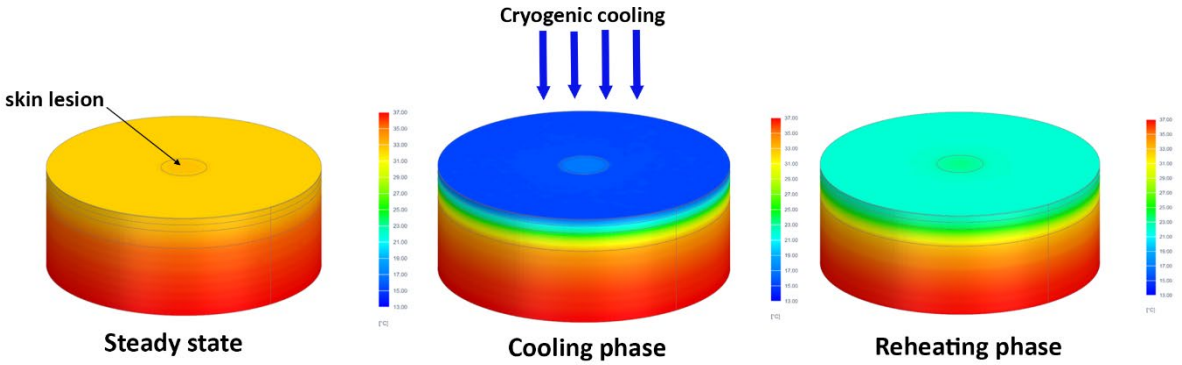

Figure 3 - Three phases of the skin model; from left to right, steady state phase, cooling phase and natural reheating phase

Table 1 gives an overview of the parameters used in this preliminary research. Properties of the skin layers are the height h_n, specific heat c_n, thermal conductivity k_n, density ρ_n, blood perfusion ω_b and metabolic heat generation Q_n. The parameters in Table 1 are from the study of Cetingül and Herman [40] based on values from literature. A 3D tetrahedral mesh type is chosen with different mesh sizes depending on the location of the mesh in the skin model. A finer mesh tends to be chosen for the most important regions for the determination of surface temperatures. The mesh sizes are shown in Figure 2.

The computational analysis consists of three phases, namely the steady-state phase, the cryogenic cooling phase and the reheating phase as shown in Figure 3. The steady state phase uses an ambient temperature of 21 °C, a blood temperature of 37 °C and a core body temperature of 37 °C. A convection heat transfer coefficient of 10 W/m²K is used, based on the properties of the ambient air. The last boundary condition is the tissue emissivity and has a value of ϵ = 0.98, determined and evaluated by Cheng and Herman [40], which can be considered as a constant value.

Layer	height h_n [mm]	specific Heat c_n $[\frac{J}{kgK}]$	thermal conductivity k_n $[\frac{W}{mK}]$	tissue density ρ_n $[\frac{kg}{m^3}]$	blood perfusion ω_b $[\frac{1}{s}]$	metabolic heat generation Q_n $[\frac{W}{m^3}]$
Epidermis [1]	0.1	3589	0.235	1200	0	0
Papillary Dermis [2]	0.7	3300	0.445	1200	0.0002	368.1
Reticular Dermis [3]	0.8	3300	0.445	1200	0.0013	368.1
Fat [4]	2	2674	0.185	1000	0.0001	368.3
Muscle [5]	8	3800	0.51	1085	0.0027	684.2
Lesion [6]	h_6= 0.2 - 1 D = 0.22 - 1.28	3852	0.558	1030	0.0063	3680

Table 1 - Nominal skin parameters used in this research according to Cetingül and Herman [37]

3. Results

3.1 In-Situ measurement head

The measurement head integrates the equipment mentioned in paragraph 2.1. It is specifically designed to allow the lesion to be cooled using the conditioned air from the Zimmer Cryo 6 cooler, while ensuring that the field of view of the macro lens remains unobstructed. Figure 4 illustrates the design of the measurement head, and the components utilized are described in section 2.1. Currently, the in-situ measurement head is undergoing thorough testing.

Preliminary results of the implemented imaging procedure can be observed in Figure 5. In its steady state, the lesion has a temperature of approximately 32 °C. Upon applying the cooling load for 60 seconds at flow level 9, the lesion's temperature decreased to around 4 °C. It should be noted that this cooling load exceeds what would be used in a clinical setting, but it is employed here to test the functionality of the in-situ measurement head. Additionally, the images display the rewarming frames at 20, 60, and 120 seconds. The skin lesion is clearly discernible in the infrared images.

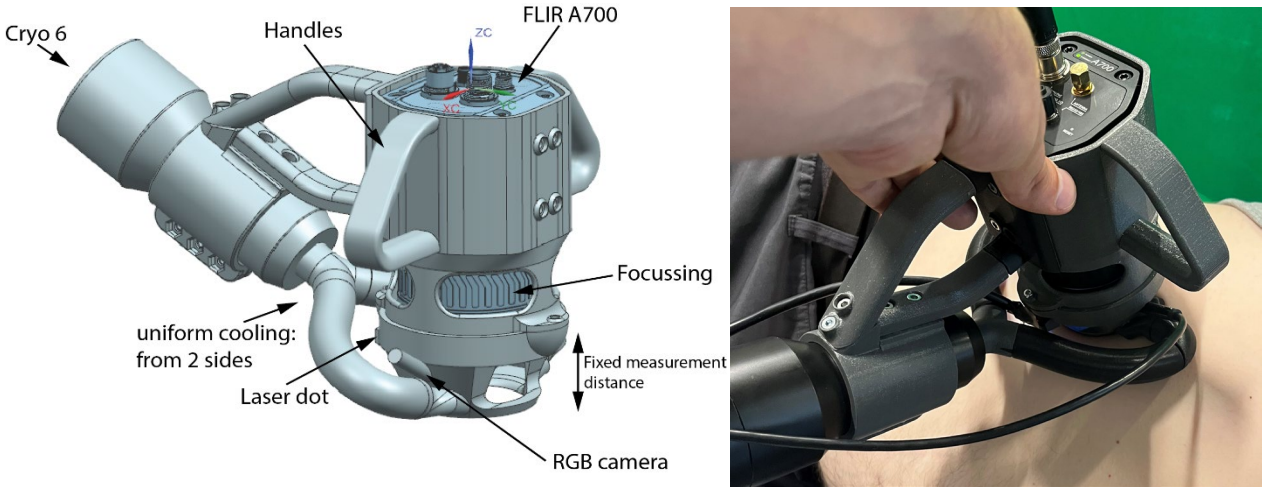

Figure 4 – (left) CAD model of the measurement head for DIRT on skin lesions, (right) in-situ measurement head during measurement

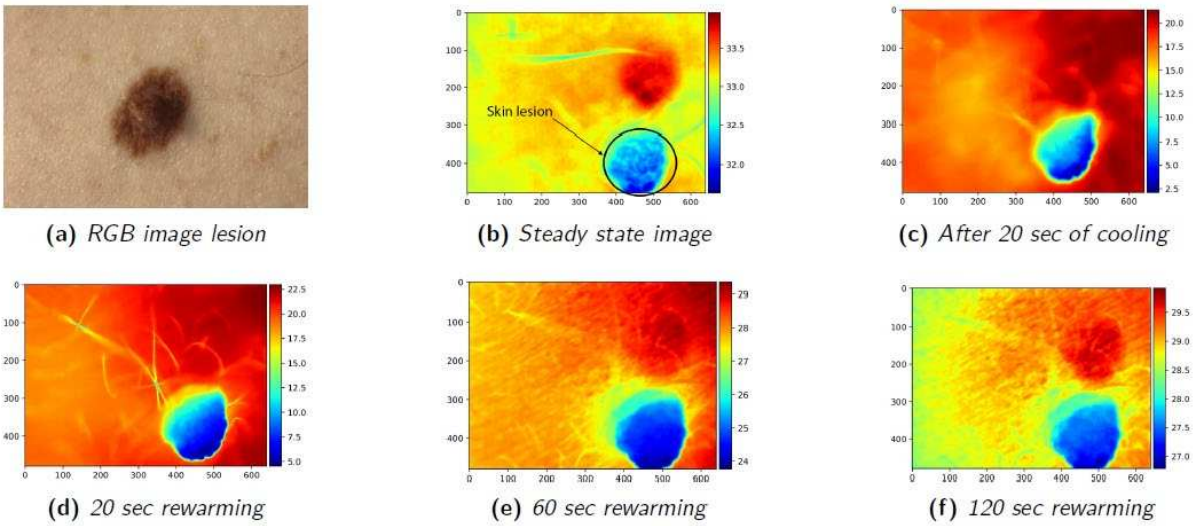

Figure 5 - RGB image and macro infrared thermography on skin lesion (20s of cooling, 120s rewarming)

3.2 Finite element skin model

Figure 6 presents the initial findings of the FEM skin model incorporating cryogenic cooling. Various cooling methods were simulated to determine the most suiTable approach for applying DIRT (Dynamic Infrared Thermography) for skin cancer diagnosis. The evaluated cooling methods included cryogenic cooling at two levels (level 1 and level 9), air cooling, constant cooling, and water cooling. Figure 7 illustrates the cooling effect of cryogenic cooling across different skin layers. Notably, the fat layer exhibits pronounced insulating properties.

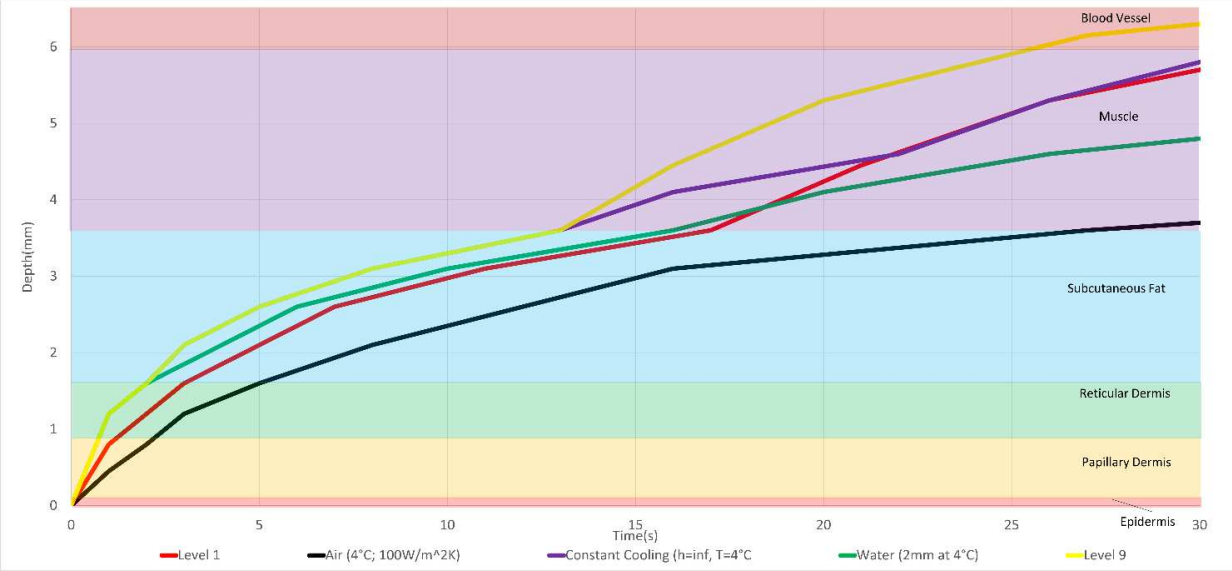

Figure 6 - Depth of cooling penetration into the skin for different cooling methods. The cryocooler is modelled at level 1 and level 9. Air cooling at 4°C, constant cooling and water cooling are included.

Two key observations emerge from the results. Firstly, higher flow levels of cryogenic cooling result in faster penetration through the skin layers. This observation holds true overall, with a particularly noTable difference between level 1 and level 9 (e.g., a 5-second disparity at the beginning of the muscle layer). Secondly, cooling at each flow level is virtually instantaneous above the epidermal layer, owing to the low thickness of the epidermis. Subsequently, as the cooling depth progresses from the start of the papillary dermis to the conclusion of the subcutaneous fat layer, the cooling rate gradually slows. This can be attributed to the varying thermal conductivity of the individual layers. Table 1 highlights the thermal conductivity disparities among the papillary dermis, reticular dermis, and subcutaneous fat layer. Specifically, the thermal conductivity of the papillary dermis and reticular dermis surpasses that of the subcutaneous fat layer. Consequently, layers with higher thermal conductivity experience faster heat transfer. Moreover, the cooling depth curve reaccelerates upon reaching the onset of the

muscle layer (i.e., the end of the subcutaneous fat layer) because the thermal conductivity of the muscle layer exceeds that of the subcutaneous fat layer.

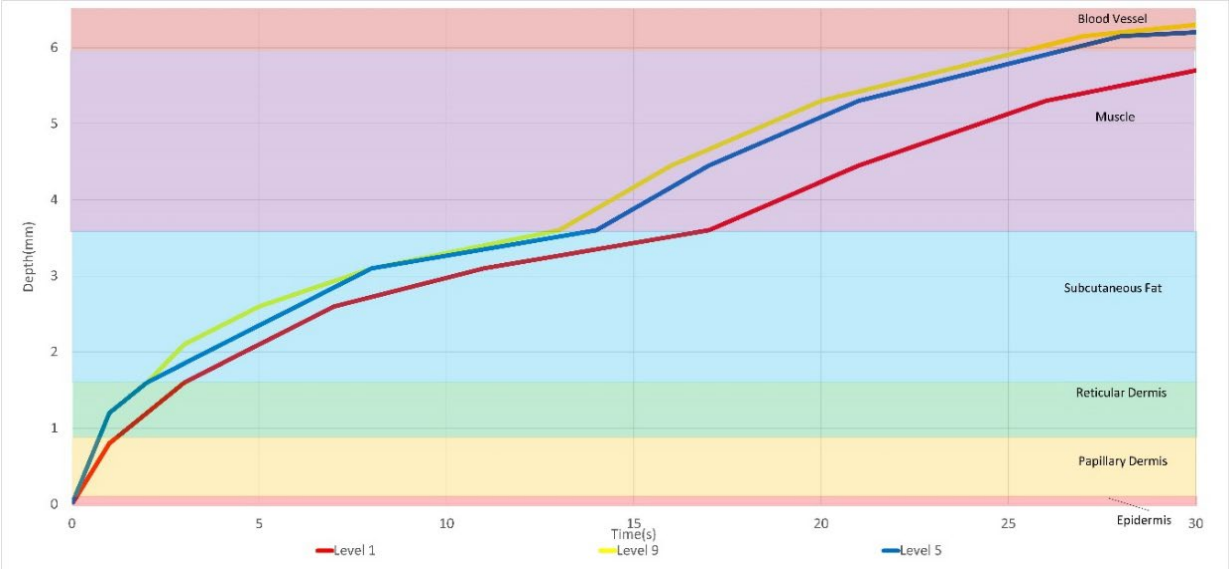

Figure 7 - Cooling depth in the skin layers in function of the time for cryogenic cooling at level 1,5 and 9

3.3 Clinical validation

In order to validate the Siemens Simcenter 3D thermal skin model, a preliminary study was conducted using a single pigmented lesion. The purpose of including only one lesion in this study was to facilitate the validation of the skin model. The lesion had a diameter of 15mm and displayed slight ulceration. The thermal response of both the skin lesion and healthy skin was measured using infrared imaging and compared with a model of the skin lesion created in Siemens Simcenter 3D. Figure 8 depicts an RGB color image of the pigmented lesion during the measurements, utilizing the measurement head described in section 3.1. The red laser dot indicates the center of the field of view for both the thermal and RGB cameras. The right image in the Figure illustrates the lesion in the thermal infrared spectrum, captured immediately after the cooling load was removed.

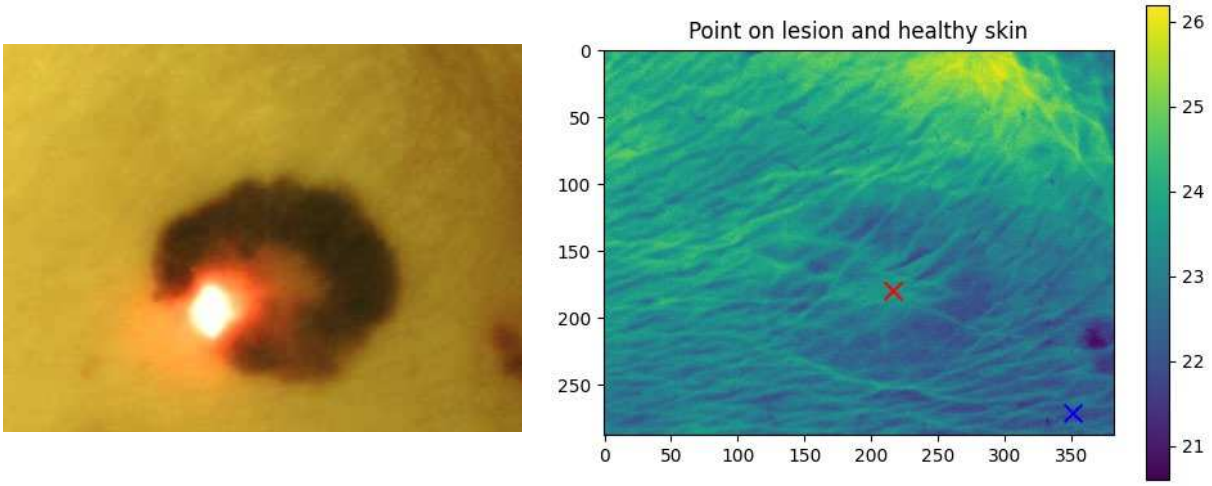

Figure 8 - (left) RGB image capturing the skin lesion, prominently displaying the red laser dot at its center, serving as a reference point within the field of view. (right) Red marker indicating the center of the lesion, while the blue marker represents the healthy skin region.

Upon applying the cooling load, the temperature of the lesion decreased to 28.59°C, while the temperature of the healthy skin was slightly lower at 27.15°C as can be seen in Figure 9. After approximately 60 seconds of reheating, the temperature of the lesion and healthy skin increased to around 33.09°C and 32.95°C, respectively. The temperature difference of more than 1°C between the lesion and healthy skin was clearly visible immediately after the cooling load was removed. However, this temperature difference gradually decreased as the reheating process continued. It should be noted that the magnitude and time evolution of this temperature difference varied based on the malignant potential of the lesion. The complete measurement cycle for the lesion and the healthy skin surrounding it is illustrated in Figure 10. The cycle begins with a 4-second steady state measurement, during which the center of the lesion exhibits a higher temperature compared to the surrounding healthy skin. Subsequently, both the lesion and healthy skin are cooled down for 20 seconds at flow level 7. It is observed that the lesion cools down to a lesser extent than the healthy skin during this cooling stage. Once the cooling load is removed, the process of reheating begins for both the lesion and healthy skin

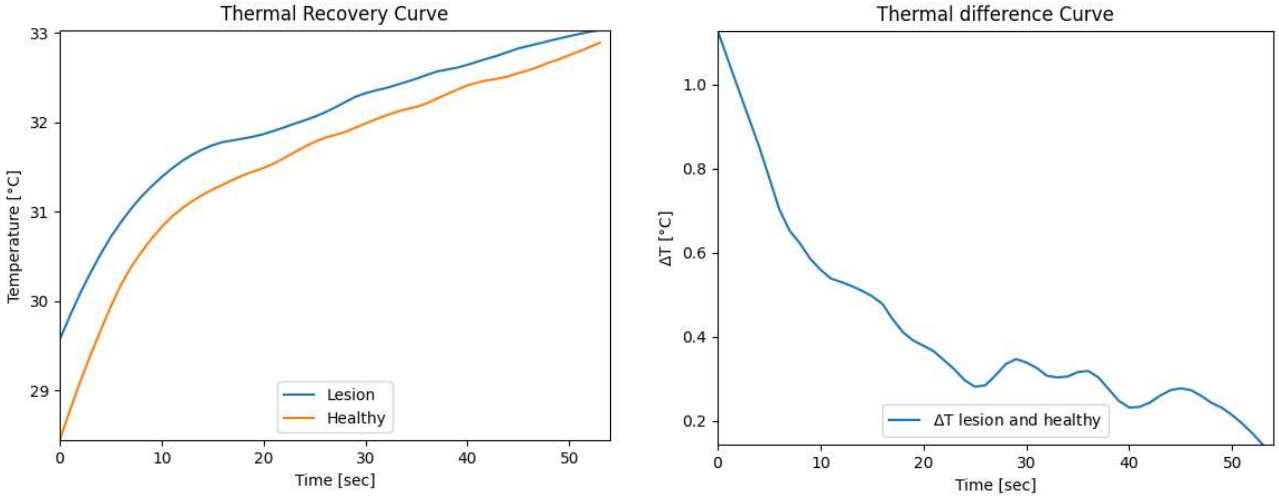

Figure 9 – (left) Time-dependent temperature profile of the pigmented lesion and healthy tissue. The lesion is denoted by the red cross, while the healthy skin is indicated by the blue cross, as shown in figure 8. (right) Thermal contrast between the lesion and healthy skin during the rewarming phase. A temperature difference exceeding 1 °C is immediately noticeable after the removal of the cooling load.

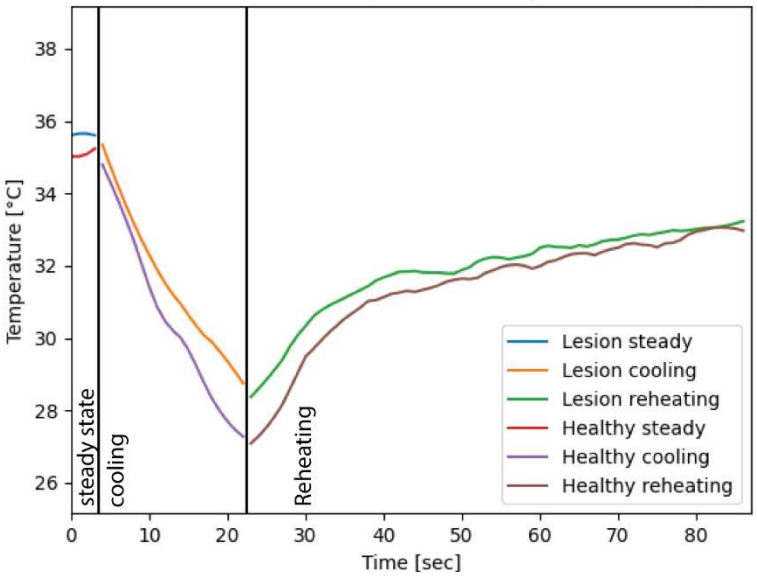

Figure 10 - Thermal curve depicting the steady state, cooling, and reheating sequences of the lesion (represented by the red cross in figure 8) and healthy skin (indicated by the blue cross in figure 8). Each sequence is captured consecutively with a slight delay, allowing for camera saving and restarting.

Input parameters for a thermal finite element model are vital in accurately simulating and predicting heat transfer behaviour within a system. These parameters include material properties such as thermal conductivity, specific heat capacity, and density, which define the thermal characteristics of the materials involved. The material parameters from Table 1 are used in this model. Geometric parameters, such as dimensions and boundary conditions, are essential for accurately representing the geometry and specifying the heat flow boundaries. The model has a diameter of 50 mm and a height of 11.8 mm. The lesion is modelled with a diameter of 15 mm and a height of 1 mm. The steady state model is shown in Figure 11: the center of the lesion and the healthy skin are depicted. Additional input parameters involve environmental factors, such as ambient temperature or radiation conditions, which can significantly influence the heat transfer process. Those parameters are listed in Table 2.

Parameter	Value	Unit
Steady state sequence	4	[seconds]
Cooling sequence	20	[seconds]
Reheating sequence	60	[seconds]
Ambient temperature	22	[°C]
Core body temperature	37	[°C]
Cryogenic cooling temperature	-30	[°C]
Air heat transfer Coefficient to room	2.5	$[W/m^2K]$
Emissivity	0.98	
Air speed at -30 °C	23.58	m/s

Table 2 – Parameters used as input for the FEM model in Siemens Simcenter 3D.

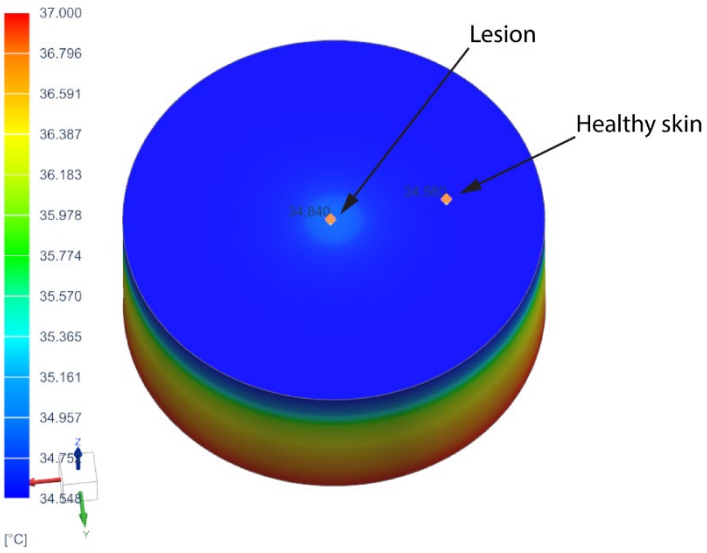

Figure 11 – Thermal model of the skin in steady state, featuring a central lesion (15mm diameter). The lesion registers a temperature of 34.84 °C, while the surrounding healthy skin exhibits a temperature of 34.56 °C.

Validating the accuracy and reliability of a thermal Finite Element Model (FEM) skin model through comparison with real data is crucial. This process involves examining the predicted thermal behaviour and temperature distribution of the FEM model and comparing it with experimental or measured data collected from real-world scenarios. In Figure 12, the thermal behaviour of the model is compared to the measurement data. Notably, during steady state, the temperature of the measured lesion and healthy skin surpasses that of the model. Throughout the cooling sequence, an interesting observation is that the model cools down at a faster rate than human skin, yet both reach the same temperature after 20 seconds of cooling. Additionally, the skin model exhibits a higher reheating rate compared to human skin, but ultimately reaches a nearly identical temperature after the 60-second mark.

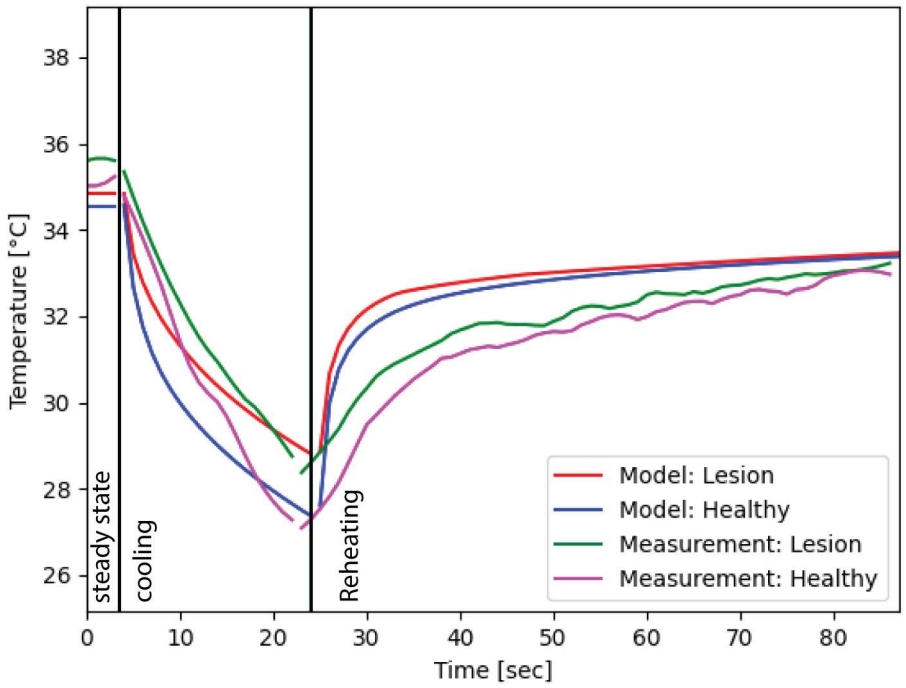

Figure 12 – Comparison of the thermal Finite Element Model (FEM) of the skin, using the parameters described in this paper, with thermal measurements on the pigmented skin lesion. Notably, the reheating rate of the model (shown in red and blue) differs from that of the pigmented lesion (depicted in green and magenta). The model exhibits overall behavior that aligns reasonably well with the measurements, although further enhancements, such as patient-specific models, could be implemented for improved accuracy.

4. Conclusion and Future work

In conclusion, skin cancer is a significant global health concern, with increasing incidence rates and a substantial impact on mortality. Early detection is crucial for improving survival rates and providing effective treatments. However, the current screening method of total body skin examination and subsequent biopsies has limitations, leading to unnecessary invasive procedures.

Dynamic infrared thermography (DIRT) has emerged as a potential non-invasive and quantitative technique for skin cancer diagnosis. By capturing thermal images and analyzing temperature variations, DIRT can detect differences in metabolic activity and angiogenesis associated with malignant skin lesions. The use of artificial intelligence and finite element models further enhances the accuracy and reliability of DIRT in diagnosing skin cancer.

A standardized measurement setup and protocol are essential for comparing measurements taken at different times. In this proof-of-concept research, a data acquisition system comprising a thermal camera, cooling device, RGB camera, laser diode, temperature and humidity sensor, and computer control was developed. The measurement hardware has undergone careful review and optimization to enhance measurement accuracy and repeatability. The system allows for consistent and accurate measurements during the DIRT procedure. Initial test measurements have yielded positive results, and the collected data is currently being processed. Although this

proof of concept for the measurement head has been successful, further adjustments to the instrument are still necessary to obtain optimal results.

When comparing the results of the finite element model and the measurements, the overall resemblance is knowledgeable. The model exhibits overall behavior that aligns reasonably well with the measurements, although further enhancements, such as patient-specific models, could be implemented for improved accuracy. The results of cooling the skin and cooling the model agree well, while there is still a difference in the heating of the real human skin and the model. Both in the model and in the measurements on the patient, a noticeable temperature difference is found between the healthy skin and the pigmented lesion. This indicates that the applied technique could possibly be used to distinguish between healthy and unhealthy skin.

By comparing various cooling techniques and durations, an optimal cooling protocol for thermal measurements of skin tissue can be identified in the future. In this work, the first steps are taken to build and validate a finite element skin model. While the basic finite element skin model in Siemens Simcenter 3D has not yet been thoroughly validated with real-life measurements, the initial findings and comparison demonstrates promising similarities to real-world scenarios. Since this study serves as a proof-of-concept, it is essential to clinically validate the cooling times. The FEM model provides an estimate of the minimum cooling time required to achieve sufficient cooling penetration. Furthermore, by making the model patient-specific, it becomes possible to customize the cooling times based on individual patients or specific anatomical locations.

Future research will focus on developing a system to mitigate uncontrolled movements of the measurement head and the patient. Additionally, efforts will be directed towards thermographic data processing, including motion tracking, image stabilization, image processing, segmentation, and lesion classification. The FEM skin model will be expanded and validated with more real-life measurements. The data generated by the FEM skin model will be used to train an AI network to be able to distinguish the healthy skin from the malign lesions.

Overall, the use of DIRT in skin cancer diagnosis shows promise in improving accuracy, reducing unnecessary biopsies, and providing a non-invasive and quantitative approach to assess malignant and non-malignant skin lesions. Further research and validation through extensive clinical studies are necessary to establish DIRT as a reliable and widely adopted tool in dermatology and skin cancer management.

Funding This research is funded by the Research Foundation-Flanders via support for the FWO research project, “Optimized skin tissue identification by combined thermal and hyperspectral imaging methodology.” (Project number 41882 (FWO G0A9720N) Jan Verstockt).

References

[1] H. Sung *et al.*, “Global Cancer Statistics 2020: GLOBOCAN Estimates of Incidence and Mortality Worldwide for 36 Cancers in 185 Countries,” *CA. Cancer J. Clin.*, vol. 71, no. 3, pp. 209–249, 2021, doi: 10.3322/caac.21660.

[2] WHO, “International Agency Research for Cancer, “Cancer WHOiafro. Estimated age-standardized incidence rates (World) in 2020, breast, woman, all ages.” http://gco.iarc.fr/today/home (accessed May 24, 2023).

[3] J. Verstockt, F. Thiessen, B. Cloostermans, W. Tjalma, and G. Steenackers, “DIEP flap breast reconstructions: thermographic assistance as a possibility for perforator mapping and improvement of DIEP flap quality,” *Appl. Opt.*, vol. 59, no. 17, p. E48, Jun. 2020, doi: 10.1364/AO.388351.

[4] M. M. Johnson *et al.*, “Skin cancer screening: recommendations for data-driven screening guidelines and a review of the US Preventive Services Task Force controversy,” *Melanoma Manag.*, vol. 4, no. 1, pp. 13–37, Mar. 2017, doi: 10.2217/mmt-2016-0022.

[5] S. G. Kandlikar *et al.*, “Infrared imaging technology for breast cancer detection – Current status, protocols and new directions,” *Int. J. Heat Mass Transf.*, vol. 108, pp. 2303–2320, May 2017, doi: 10.1016/j.ijheatmasstransfer.2017.01.086.

[6] A. Brunssen, A. Waldmann, N. Eisemann, and A. Katalinic, “Impact of skin cancer screening and secondary prevention campaigns on skin cancer incidence and mortality: A systematic review,” *J. Am. Acad. Dermatol.*, vol. 76, no. 1, pp. 129-139.e10, Jan. 2017, doi: 10.1016/j.jaad.2016.07.045.

[7] R. P. Braun, M. Oliviero, I. Kolm, L. E. French, A. A. Marghoob, and H. Rabinovitz, “Dermoscopy: what’s new?,” *Clin. Dermatol.*, vol. 27, no. 1, pp. 26–34, Jan. 2009, doi: 10.1016/j.clindermatol.2008.09.003.

[8] M. e. Vestergaard, P. Macaskill, P. e. Holt, and S. w. Menzies, “Dermoscopy compared with naked eye examination for the diagnosis of primary melanoma: a meta-analysis of studies performed in a clinical setting,” *Br. J. Dermatol.*, vol. 159, no. 3, pp. 669–676, 2008, doi: 10.1111/j.1365-2133.2008.08713.x.

[9] S. E. Godoy *et al.*, “Dynamic infrared imaging for skin cancer screening,” *Infrared Phys. Technol.*, vol. 70, pp. 147–152, May 2015, doi: 10.1016/j.infrared.2014.09.017.

[10] M. P. Çetingül and C. Herman, “Quantification of the thermal signature of a melanoma lesion,” *Int. J. Therm. Sci.*, vol. 50, no. 4, pp. 421–431, Apr. 2011, doi: 10.1016/j.ijthermalsci.2010.10.019.

[11] M. Bonmarin and F. A. Le Gal, “Chapter 31 - Thermal Imaging in Dermatology,” in *Imaging in Dermatology*, M. R. Hamblin, P. Avci, and G. K. Gupta, Eds., Boston: Academic Press, 2016, pp. 437–454. doi: 10.1016/B978-0-12-802838-4.00031-5.

[12] K. L. Williams, “Infrared Thermometry as a Tool in Medical Research,” *Ann. N. Y. Acad. Sci.*, vol. 121, no. 1, pp. 99–112, 1964, doi: 10.1111/j.1749-6632.1964.tb13689.x.
[13] B. F. Jones, “A reappraisal of the use of infrared thermal image analysis in medicine,” *IEEE Trans. Med. Imaging*, vol. 17, no. 6, pp. 1019–1027, Dec. 1998, doi: 10.1109/42.746635.
[14] A. Nowakowski and M. Kaczmarek, “Active Dynamic Thermography - Problems of implementation in medical diagnostics,” *Quant. InfraRed Thermogr. J.*, vol. 8, no. 1, pp. 89–106, Jun. 2011, doi: 10.3166/qirt.8.89-106.
[15] B. B. Lahiri, S. Bagavathiappan, T. Jayakumar, and J. Philip, “Medical applications of infrared thermography: A review,” *Infrared Phys. Technol.*, vol. 55, no. 4, pp. 221–235, Jul. 2012, doi: 10.1016/j.infrared.2012.03.007.
[16] F. E. F. Thiessen *et al.*, “Dynamic infrared thermography (DIRT) in Deep Inferior Epigastric Perforator (DIEP) flap breast reconstruction: standardization of the measurement set-up,” *Gland Surg.*, vol. 8, no. 6, pp. 799–805, Dec. 2019, doi: 10.21037/gs.2019.12.09.
[17] F. E. F. Thiessen *et al.*, “Dynamic Infrared Thermography (DIRT) in DIEP flap breast reconstruction: A clinical study with a standardized measurement setup,” *Eur. J. Obstet. Gynecol. Reprod. Biol.*, vol. 252, pp. 166–173, Sep. 2020, doi: 10.1016/j.ejogrb.2020.05.038.
[18] F. E. F. Thiessen *et al.*, “Dynamic Infrared Thermography (DIRT) in DIEP-flap breast reconstruction: A review of the literature,” *Eur. J. Obstet. Gynecol. Reprod. Biol.*, vol. 242, pp. 47–55, Nov. 2019, doi: 10.1016/j.ejogrb.2019.08.008.
[19] J. C. Torres-Galván, E. Guevara, E. S. Kolosovas-Machuca, A. Oceguera-Villanueva, J. L. Flores, and F. J. González, “Deep convolutional neural networks for classifying breast cancer using infrared thermography,” *Quant. InfraRed Thermogr. J.*, vol. 19, no. 4, pp. 283–294, Aug. 2022, doi: 10.1080/17686733.2021.1918514.
[20] M. Kaczmarek, A. Nowakowski, M. Suchowirski, J. Siebert, and W. Stojek, “Active dynamic thermography in cardiosurgery,” *Quant. InfraRed Thermogr. J.*, vol. 4, no. 1, pp. 107–123, Jun. 2007, doi: 10.3166/qirt.4.107-123.
[21] A. S. Hakim and R. N. Awale, “Extraction of hottest blood vessels from breast thermograms using state-of-the-art image segmentation methods,” *Quant. InfraRed Thermogr. J.*, vol. 19, no. 5, pp. 347–365, Oct. 2022, doi: 10.1080/17686733.2021.1974209.
[22] A. Özdil and B. Yılmaz, “Automatic body part and pose detection in medical infrared thermal images,” *Quant. InfraRed Thermogr. J.*, vol. 19, no. 4, pp. 223–238, Aug. 2022, doi: 10.1080/17686733.2021.1947595.
[23] J. Verstockt, S. Verspeek, F. Thiessen, W. A. Tjalma, L. Brochez, and G. Steenackers, “Skin Cancer Detection Using Infrared Thermography: Measurement Setup, Procedure and Equipment,” *Sensors*, vol. 22, no. 9, Art. no. 9, Jan. 2022, doi: 10.3390/s22093327.
[24] N. Akhter, R. Manza, S. Shaikh, B. Gawali, P. Yannawar, and S. Shaikh, “Diagnosis of Melanoma Using Thermography: A Review,” presented at the International Conference on Applications of Machine Intelligence and Data Analytics (ICAMIDA 2022), Atlantis Press, May 2023, pp. 466–473. doi: 10.2991/978-94-6463-136-4_40.
[25] C. Magalhaes, J. M. R. S. Tavares, J. Mendes, and R. Vardasca, “Comparison of machine learning strategies for infrared thermography of skin cancer,” *Biomed. Signal Process. Control*, vol. 69, p. 102872, Aug. 2021, doi: 10.1016/j.bspc.2021.102872.
[26] C. Magalhaes, J. Mendes, and R. Vardasca, “Meta-Analysis and Systematic Review of the Application of Machine Learning Classifiers in Biomedical Applications of Infrared Thermography,” *Appl. Sci.*, vol. 11, no. 2, Art. no. 2, Jan. 2021, doi: 10.3390/app11020842.
[27] C. Magalhaes, J. Mendes, and R. Vardasca, “The role of AI classifiers in skin cancer images,” *Skin Res. Technol.*, vol. 25, no. 5, pp. 750–757, 2019, doi: 10.1111/srt.12713.
[28] H. Chen, K. Wang, Z. Du, W. Liu, and Z. Liu, “Predicting the thermophysical properties of skin tumor based on the surface temperature and deep learning,” *Int. J. Heat Mass Transf.*, vol. 180, p. 121804, Dec. 2021, doi: 10.1016/j.ijheatmasstransfer.2021.121804.
[29] A. Kirimtat, O. Krejcar, and A. Selamat, “A Mini-review of Biomedical Infrared Thermography (B-IRT),” in *Bioinformatics and Biomedical Engineering*, I. Rojas, O. Valenzuela, F. Rojas, and F. Ortuño, Eds., in Lecture Notes in Computer Science, vol. 11466. Cham: Springer International Publishing, 2019, pp. 99–110. doi: 10.1007/978-3-030-17935-9_10.
[30] H. Qi and N. Diakides, “Infrared imaging in medicine,” University of Tennessee, 2007.
[31] Y. Y. Lee *et al.*, “Surrogate human sensor for human skin surface temperature measurement in evaluating the impacts of thermal behaviour at outdoor environment,” *Measurement*, vol. 118, pp. 61–72, Mar. 2018, doi: 10.1016/j.measurement.2018.01.010.
[32] W. Minkina and S. Dudzik, *Infrared Thermography - Errors and Uncertainties*, 1st ed. Wiley, 2009.
[33] T. M. Buzug, S. Schumann, L. Pfaffmann, U. Reinhold, and J. Ruhlmann, “Functional infrared imaging for skin-cancer screening,” in *Annual International Conference of the IEEE Engineering in Medicine and Biology - Proceedings*, 2006, pp. 2766–2769. doi: 10.1109/IEMBS.2006.259895.
[34] J. H. Flores-Sahagun, J. V. C. Vargas, and F. A. Mulinari-Brenner, “Analysis and diagnosis of basal cell carcinoma (BCC) via infrared imaging,” *Infrared Phys. Technol.*, vol. 54, no. 5, pp. 367–378, Sep. 2011, doi: 10.1016/j.infrared.2011.05.002.
[35] G. Santulli, *Angiogenesis: Insights from a Systematic Overview*. Nova Publisher, 2013.
[36] R. S. Kerbel, “Tumor Angiogenesis,” *N. Engl. J. Med.*, vol. 358, no. 19, pp. 2039–2049, May 2008, doi: 10.1056/NEJMra0706596.
[37] D. Elder, “Tumor Progression, Early Diagnosis and Prognosis of Melanoma,” *Acta Oncol.*, vol. 38, no. 5, pp. 535–548, Jan. 1999, doi: 10.1080/028418699431113.
[38] F. J. González, C. Castillo-Martínez, R. Valdes-Rodríguez, E. S. Kolosovas-Machuca, U. Villela-Segura, and B. Moncada, “Thermal signature of melanoma and non-melanoma skin cancers,” in *Proceedings of the 2012 International Conference on Quantitative InfraRed Thermography*, QIRT Council, 2012. doi: 10.21611/qirt.2012.276.

[39] L. J. Jiang *et al.*, “A perspective on medical infrared imaging,” *J. Med. Eng. Technol.*, vol. 29, no. 6, pp. 257–267, Jan. 2005, doi: 10.1080/03091900512331333158.
[40] M. P. Çetingül and C. Herman, “A heat transfer model of skin tissue for the detection of lesions: Sensitivity analysis,” *Phys. Med. Biol.*, vol. 55, no. 19, pp. 5933–5951, Oct. 2010, doi: 10.1088/0031-9155/55/19/020.
[41] D. A. Torvi and J. D. Dale, “A Finite Element Model of Skin Subjected to a Flash Fire,” *J. Biomech. Eng.*, vol. 116, no. 3, pp. 250–255, Aug. 1994, doi: 10.1115/1.2895727.
[42] M. P. Çetingül and C. Herman, “Transient Thermal Response of Skin Tissue,” presented at the ASME 2008 Heat Transfer Summer Conference collocated with the Fluids Engineering, Energy Sustainability, and 3rd Energy Nanotechnology Conferences, American Society of Mechanical Engineers Digital Collection, Jul. 2009, pp. 355–361. doi: 10.1115/HT2008-56409.
[43] P. Buliński, W. Adamczyk, and Z. Ostrowski, “Bioheat Transfer Model with Active Thermoregulation: Sensitivity of Temperature Field on Tissue Properties,” in *Innovations in Biomedical Engineering*, M. Gzik, E. Tkacz, Z. Paszenda, and E. Piętka, Eds., in Advances in Intelligent Systems and Computing. Cham: Springer International Publishing, 2017, pp. 259–266. doi: 10.1007/978-3-319-47154-9_30.
[44] Z. Ostrowski, P. Buliński, W. Adamczyk, P. Kozołub, and A. Nowak, “Numerical model of heat transfer in skin lesions,” *Sci. Lett. Univ. Rzesz. Technol. - Mech.*, vol. 32, no. 87(1/2015), pp. 55–62, 2015, doi: 10.7862/rm.2015.6.
[45] S. K. Kandala, D. Deng, and C. Herman, “Simulation of Discrete Blood Vessel Effects on the Thermal Signature of a Melanoma Lesion,” in *Volume 3B: Biomedical and Biotechnology Engineering*, San Diego, California, USA: American Society of Mechanical Engineers, Nov. 2013, p. V03BT03A038. doi: 10.1115/IMECE2013-64451.
[46] P. Wongchadakul and P. Rattanadecho, “Mathematical Modeling of Multilayered Skin with Embedded Tumor Through Combining Laser Ablation and Nanoparticles: Effects of Laser Beam Area, Wavelength, Intensity, Tumor Absorption Coefficient and Its Position,” *Int. J. Heat Technol.*, vol. 39, no. 1, pp. 89–100, Feb. 2021, doi: 10.18280/ijht.390109.
[47] M. Strąkowska and B. Więcek, “Thermal modeling of planar and cylindrical biomedical multilayers structures in frequency domain,” *Meas. Autom. Monit.*, no. Vol. 65, No. 2, pp. 32--36, 2019.
[48] T. C. Barros and A. A. A. Figueiredo, “Three-dimensional numerical evaluation of skin surface thermal contrast by application of hypothermia at different depths and sizes of the breast tumor,” *Comput. Methods Programs Biomed.*, vol. 236, p. 107562, Jun. 2023, doi: 10.1016/j.cmpb.2023.107562.
[49] C. Hildebrandt, C. Raschner, and K. Ammer, “An Overview of Recent Application of Medical Infrared Thermography in Sports Medicine in Austria,” *Sensors*, vol. 10, no. 5, Art. no. 5, May 2010, doi: 10.3390/s100504700.
[50] W. Shen, J. Zhang, and F. Yang, “Modeling and numerical simulation of bioheat transfer and biomechanics in soft tissue,” *Math. Comput. Model.*, vol. 41, no. 11–12, pp. 1251–1265, May 2005, doi: 10.1016/j.mcm.2004.09.006.
[51] H. H. Pennes, “Analysis of tissue and arterial blood temperatures in the resting human forearm. 1948.,” *J. Appl. Physiol.*, 1948, doi: 10.1152/JAPPL.1948.1.2.93.
[52] L. Zhu, “Chapter 2 Heat Transfer applications in Biological Systems,” *McGraw-Hill Educ.*, vol. Volume 1, no. Biomedical Engineering and Design Handbook, 2010, Accessed: May 19, 2022. [Online]. Available: https://www.semanticscholar.org/paper/CHAPTER-2-HEAT-TRANSFER-APPLICATIONS-IN-BIOLOGICAL-Zhu/a56e3ec383e867de9956eac63f00645c39356047
[53] N. Sarkar, “A novel Pennes’ bioheat transfer equation with memory-dependent derivative,” *Math. Models Eng.*, vol. 2, no. 2, pp. 151–157, Dec. 2016, doi: 10.21595/mme.2016.18024.
[54] “MDCG 2021-24 - Guidance on classification of medical devices.” https://ec.europa.eu/health/latest-updates/mdcg-2021-24-guidance-classification-medical-devices-2021-10-04_en (accessed May 11, 2022).
[55] “Cryo 6 Brochure - Information About the Zimmer Skin Cooling Chiller,” *Zimmer MedizinSystems*. https://zimmerusa.com/products/cryo-therapy/cryo-6/cryo-6-brochure/ (accessed May 11, 2022).
[56] R. Vardasca, L. Vaz, and J. Mendes, “Classification and Decision Making of Medical Infrared Thermal Images,” in *Classification in BioApps*, N. Dey, A. S. Ashour, and S. Borra, Eds., in Lecture Notes in Computational Vision and Biomechanics, vol. 26. Cham: Springer International Publishing, 2018, pp. 79–104. doi: 10.1007/978-3-319-65981-7_4.
[57] M. P. Çetingül and C. Herman, “A heat transfer model of skin tissue for the detection of lesions: sensitivity analysis,” *Phys. Med. Biol.*, vol. 55, no. 19, pp. 5933–5951, Sep. 2010, doi: 10.1088/0031-9155/55/19/020.
[58] J. Iljaž, L. C. Wrobel, M. Hriberšek, and J. Marn, “Numerical modelling of skin tumour tissue with temperature-dependent properties for dynamic thermography,” *Comput. Biol. Med.*, vol. 112, p. 103367, Sep. 2019, doi: 10.1016/j.compbiomed.2019.103367.

Rebuttal: Finite element skin models as additional data for dynamic infrared thermography on skin lesions

Comments:

1) Abstract: “conducted at the University of Antwerp. -> “conducted at the University of Antwerp (Belgium).”
    a. Adapted

2) Section 1.2.: “but can be found in a previous contribution [20], [21].” -> “but can be found in previous contributions [20], [21].”
    a. Adapted
3) Section 3.3.: “Figure 3 depicts an RGB color…” -> Are you referring to Fig. 8?
    a. Adapted
4) It seems Fig. 9 has not been described/cited in the text.
    a. Adapted
5) Caption of Fig. 9: “…the blue cross, as shown in figure 3.”Again, are you referring to Fig. 8?
    a. Adapted
6) In the caption of Fig. 10 please indicate that you are referring to Fig. 8 talking about red and blue crosses.
    a. Adapted
7) Section 4 is more oriented towards future perspectives (several) then in describing the conclusions of this work. Please make the conclusions (focused on the results obtained) more of impact for the reader.
    a. Added an extra paragraph about the comparison between the measurements.
8) I would like to call your attention to the crucial importance of recent citations besides the original sources to present the relevant and substantial literature background of a paper published in the Quantitative InfraRed Thermography Journal.
    a. Added references to the QIRT journal
9) Table 2 has a slightly different layout compared to Table 1. Please adopt only one.
    a. The 2nd table is presented a bit larger. The layout is, to my opinion the same. The lines and text are bold at the same locations.
10) Captions of Figures are different from what is commonly adopt. You are using a gray font. Please use the same you use in the first version of the manuscript.
    a. Adapted
11) Finally, when referring Table and Figure in the text, please use capital letter. E.g., “As it can be seen in Figure 14…”
    a. Adapted